Microscale anatomy of the 1999 Chi-Chi earthquake fault zone

Anne-Marie Boullier, En-Chao Yeh, Sebastien Boutareaud, Sheng-Rong Song, Chin-Ho Tsai

Geochemistry Geophysics Geosystems G3
AN ELECTRONIC JOURNAL OF THE EARTH SCIENCES
Published by AGU and the Geochemical Society

Article
Volume 10, Number 3
31 March 2009
Q03016, doi:10.1029/2008GC002252
ISSN: 1525-2027

Microscale anatomy of the 1999 Chi-Chi earthquake fault zone

Anne-Marie Boullier
Laboratoire de Géophysique Interne et Tectonophysique, Université Joseph Fourier, CNRS, Maison des Géosciences, BP 53, F-38041 Grenoble CEDEX 9, France (anne-marie.boullier@obs.ujf-grenoble.fr)

En-Chao Yeh
Department of Geosciences, National Taiwan University, 1 Roosevelt Road, Section 4, Taipei 106, Taiwan

Sébastien Boutareaud
Laboratoire de Géophysique Interne et Tectonophysique, Université Joseph Fourier, CNRS, Maison des Géosciences, BP 53, F-38041 Grenoble CEDEX 9, France

Sheng-Rong Song
Department of Geosciences, National Taiwan University, 1 Roosevelt Road, Section 4, Taipei 106, Taiwan

Chin-Ho Tsai
Institute of Earth Sciences, Meilun Campus, National Dong Hwa University, 123 Hua-Hsi Road, Hualien 970, Taiwan

[1] Two TCDP boreholes A and B were drilled in the northern part of the Chelungpu thrust fault where the Chi-Chi earthquake (21 September 1999, Mw 7.6) showed large displacement, low ground acceleration, and high slip velocity. In this paper, we describe the microstructures of the Chi-Chi Principal Slip Zone (PSZ) within black gouges localized at 1111 m depth in Hole A and at 1136 m depth in Hole B. In the FZA1111 the PSZ is a 2 cm-thick isotropic clay-rich gouge which contains aggregates formed by central clasts coated by clay cortex (clay-clast aggregates (CCAs)) and fragments of older gouges segregated in the top third of the PSZ. In FZB1136 the PSZ is 3 mm thick and is characterized by a foliated gouge displaying an alternation of clay-rich and clast-rich layers. The presence of CCAs, plucked underlying gouge fragments, gouge injections, and the occurrence of reverse grain size segregation of large clasts in the FZA1111 isotropic gouge suggest that the gouge was fluidized as a result of frictional heating and thermal pressurization. The foliated gouge in FZB1136 may be one locus of strain localization and related heat production. Small calcite veins present above the isotropic FZA1111 PSZ gouge and, characterized by an increasing strain with increasing distance away from the PSZ, are attributed to coseismic fluid escape from the pressurized gouge. The observed microstructures are interpreted in view of their seismic implications for the Chi-Chi earthquake in terms of slip weakening mechanisms by thermal pressurization, gouge fluidization, coseismic fluid distribution, and postseismic slip. Above the PSZ, several layers of compacted gouges containing deformed CCAs and gouge fragments correspond to several PSZ of past earthquakes similar to the Chi-Chi earthquake and display a fault-parallel cleavage resulting from a low strain rate pressure solution deformation mechanism that may be correlated to the interseismic periods.

Components: 14,416 words, 12 figures, 2 tables.

Keywords: Chi-Chi earthquake; principal slip zone; microstructures; gouge fluidization; clay-clast aggregates; TCDP.

Index Terms: 8030 Structural Geology: Microstructures; 8163 Tectonophysics: Rheology and friction of fault zones (8034); 8045 Structural Geology: Role of fluids.

Received 19 September 2008; **Revised** 22 December 2008; **Accepted** 15 January 2009; **Published** 31 March 2009.

Boullier, A.-M., E.-C. Yeh, S. Boutareaud, S.-R. Song, and C.-H. Tsai (2009), Microscale anatomy of the 1999 Chi-Chi earthquake fault zone, *Geochem. Geophys. Geosyst.*, *10*, Q03016, doi:10.1029/2008GC002252.

1. Introduction

[2] Over the last 10 years several international drilling and coring programs have been conducted through active faults to better understand earthquakes (see *Zoback et al.* [2007] for a review). Most of them have been conducted after major earthquakes and through different types of rocks, granodiorite in the Nojima fault (Kobe earthquake, 1995, Hirabayashi borehole, Japan [*Ohtani et al.*, 2000; *Tanaka et al.*, 2001]), calcareous and detrital formations in the Corinth rift (Corinth Rift Laboratory, Greece [*Cornet et al.*, 2004]), sandstone and siltstone alternations in the Chelungpu fault (Chi-Chi earthquake, 1999, Taiwan Chelungpu fault Drilling Project [*Song et al.*, 2007; *Hung et al.*, 2007]), and arkoses, shales, siltstones, and serpentines in the San Andreas fault (Parkfield earthquake, 2004, San Andreas Fault Observatory at Depth, California [*Hickman et al.*, 2004; *Zoback et al.*, 2007]). They correspond also to different tectonic contexts, such as reverse dextral strike slip, normal, thrust, and dextral strike-slip faults, respectively. Therefore, each drill hole provides specific but complementary data for the international earthquake community which has considerably benefited from multidisciplinary approaches on these boreholes and core samples.

[3] The Chi-Chi earthquake (21 September 1999, Mw = 7.6) produced a surface rupture of 80 km, and up to 10 m offset on the northern part of the Chelungpu thrust fault [*Kao and Chen*, 2000; *Chen et al.*, 2001a; *Yu et al.*, 2001]. It was recorded by the very dense Taiwan Strong Motion and GPS Networks allowing models of spatial slip distribution [*Ma et al.*, 2001], determination of rupture velocity [*Chen et al.*, 2001b], coseismic and postseismic deformation [*Pathier et al.*, 2003; *Yu et al.*, 2003]. The Taiwan Chelungpu Fault Drilling Project (TCDP) started in 2002 and drilled two vertical boreholes 40 m apart (2000.3 m deep Hole A and 1352.6 m deep Hole B), about 2 km east of the surface rupture, near the town of DaKeng (Figure 1). The TCDP location was chosen because of large displacement, low ground acceleration, and high slip velocity in the northern part of the surface rupture, in contrast to the smaller displacement and higher accelerations in the southern part [*Ma et al.*, 2003]. To explain such a behavior, *Ma et al.* [2003] have proposed the elastohydrodynamic lubrication model [*Brodsky and Kanamori*, 2001] in which a high fluid pressure is generated in a fluidized gouge during slip. However, frictional heating represents another possible mechanism for inducing thermal pressurization in a slip zone [*Sibson*, 1973; *Lachenbruch*, 1980; *Wibberley and Shimamoto*, 2005] and has been proposed also for the Chi-Chi Principal Slip Zone (PSZ) [*Sibson*, 2003] by some authors [*Tanaka et al.*, 2006, 2007]. However, no textural evidence has been found yet for any of these mechanisms in the Chi-Chi PSZ.

[4] In this paper we present a detailed microstructural analysis of gouge core samples from TCDP boreholes A and B. First, we focus on microstructures of a very localized gouge zone, which is interpreted to be the Chi-Chi PSZ [*Ma et al.*, 2006], and specify the most likely slip weakening mechanism that occurred during the earthquake. Second, we describe the microstructures within the fault zone and interpret them in terms of deformation and fluid-rock interactions related to different stages of past seismic cycles on the Chelungpu thrust fault.

2. Tectonic Setting and Geological Background

[5] The Taiwan mountain belt is the result of an oblique convergent boundary and complex subduction reversal (Figure 1a insert) between the Eurasian and Philippine Sea Plates [*Chai*, 1972; *Ho*, 1986; *Teng*, 1990; *Wu et al.*, 1997a; *Lallemand et al.*, 2001], which has led to active faulting and intense crustal deformation, as indicated by frequent earthquakes. The boundary between the western coastal plain and the western foothills [*Ho*, 1988] is one of the most active regions within Taiwan. Several disastrous earthquakes have occurred along this boundary, including the 1999 Chi-Chi earthquake

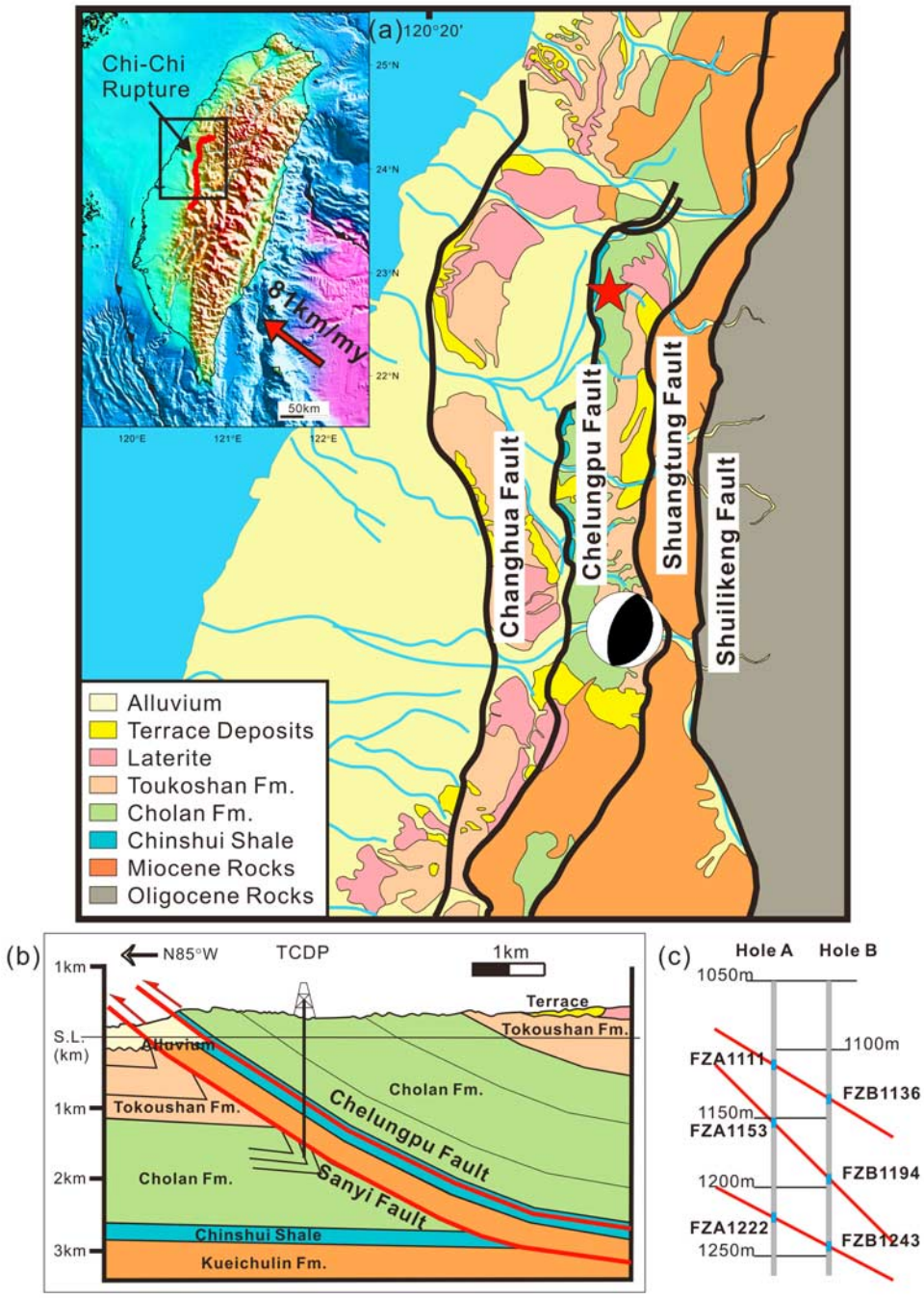

Figure 1. Geological map and cross section of the fold and thrust belt of western Taiwan. The insert shows the geodynamical context of Taiwan. (a) Geological map, distribution of the major thrusts of western Taiwan. The focal mechanism of the Chi-Chi earthquake is located at the hypocenter [*Kao and Chen*, 2000]. The TCDP site is indicated by the red star. (b) Cross section through the drill site indicating the principal sedimentary formations and the principal faults [after *Hung et al.*, 2007]. (c) Correlation between the different fault zones observed in Holes A and B after *Hirono et al.* [2007b].

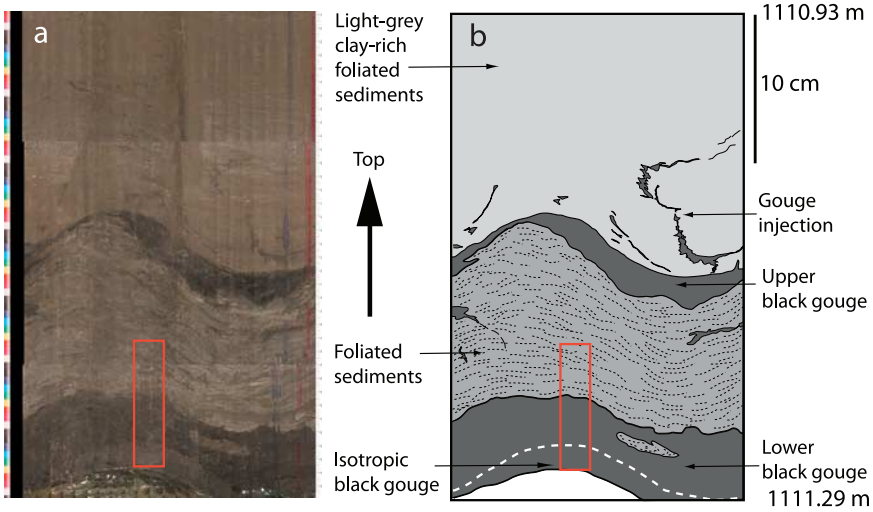

Figure 2. (a) Unrolled scanning image of FZA1111 and (b) corresponding sketch showing the principal structural characteristics of the fault zone and the location (red box) of the thin section shown in Figure 3.

[*Wang et al.*, 2000]. The stratigraphic formations in this active region (Figure 1a) are late Miocene to Pliocene marine sediments characterized by alternating sandstone, siltstone and shales, and Pleistocene fluvial to shallow marine sediments with alternating conglomerates, sandstones, and siltstones [*Ho*, 1988; *Song et al.*, 2007]. These formations are crosscut and tectonically stacked by three bedding-parallel major faults (Figure 1a) that form a west-verging ramp flat system [*Yue et al.*, 2005]. Among these faults, the Chelungpu fault zone played the major role in the Chi-Chi earthquake. From reconstruction of balanced cross sections, *Yue et al.* [2005] determined a total displacement of about 14 km for the Chelungpu thrust system and 0.3 km total slip on a newly propagated North Chelungpu Chinshui detachment where the Chi-Chi earthquake occurred (Figure 1b). The TCDP is located in the northern part of the fault where the maximum seismic displacement was measured.

[6] Several fault zones were crossed by TCDP Hole A and Hole B [*Yeh et al.*, 2007; *Hirono et al.*, 2007b]. Lithological and mineralogical descriptions, as well as the physical properties of the core and shear zones, have already been presented [*Song et al.*, 2007; *Yeh et al.*, 2007; *Hirono et al.*, 2007b, 2008]. Only FZA1111 (Hole A, Fault Zone at 1111 m depth) and FZB1136 (Hole B, Fault Zone at 1136 m depth) are described in this paper because they have been recognized as corresponding to the Chi-Chi earthquake fault zone [*Ma et al.*, 2006; *Song et al.*, 2007; *Hirono et al.*, 2008] and to the North Chelungpu Chinshui detachment [*Yue et al.*, 2005].

3. Structures of TCDP FZA1111 and FZB1136

[7] Core samples of these fault zones are limited in volume. They are also difficult to work with because they are rich in swelling clay minerals and poorly consolidated. Therefore, nondestructive techniques such as optical petrography, scanning electron microscopy (SEM), and X ray fluorescence (XRF) element mapping were selected to analyze extremely challenging polished thin or thick sections of FZA1111 and FZB1136.

3.1. FZA 1111

[8] The FZA1111 is a bedding-parallel thrust (30° dip) developed within siltstone-dominated sediments. The damage zone is thicker in the hanging wall than the footwall (2.85 m versus 0.2 m), and several subzones have been macroscopically defined on the drill site [*Yeh et al.*, 2007; *Sone et al.*, 2007a]. In this paper we will focus on the fault core and its immediate vicinity (Figure 2). We will refer to deformed sediments as representing the rocks in which fossils, sedimentary layering, and detrital mica grains are still present, and gouges the rocks in which none of these structures could be recognized.

[9] Several macroscopic features were encountered in FZA1111 from top to bottom (Figure 2), and these are mentioned in the following detailed

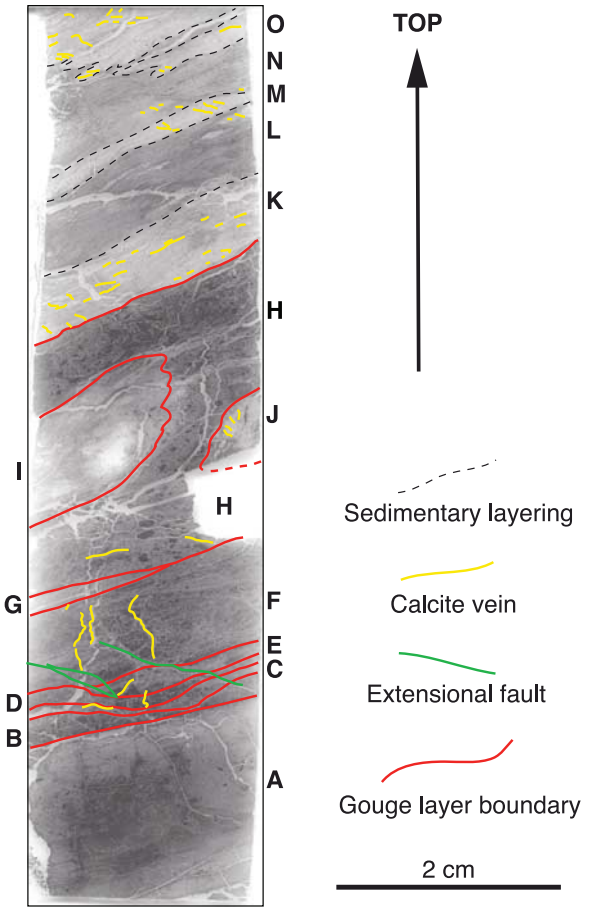

Figure 3. Scan of the thin section with line drawings indicating the limits of the principal layers A to O, calcite veins, small extensional faults, and transposed sedimentary layering.

descriptions: (1) thin jigsaw lines of fine-grained black material crosscut the cleavage of light gray clay-rich foliated sediments with an average subvertical attitude [*Yeh et al.*, 2007; *Sone et al.*, 2007a]; (2) an upper foliated thin black gouge with a straight upper boundary and a wavy lower boundary; (3) a lower black gouge with an irregular upper boundary with the foliated sediments but a sharp and straight lower contact corresponding to a 2 cm thick homogeneous and isotropic black gouge; (4) a solid disk of black material made of ultracataclasites, referred to as black disk in the TCDP literature and hereafter, and situated below the black gouge. The upper half of this black disk was accidentally broken during core handling and only fragments could be observed. The lower half of the black disk shows a clear 70°SW slickenside [*Yeh et al.*, 2007], which is consistent with the slip direction of the Chi-Chi earthquake obtained from seismic data inversion [*Ma et al.*, 2001]. These compacted hard black disks are compacted ultracataclasites similar to the hard black disks described in FZB1194 and FZB1243 by *Hirono et al.* [2006a] and interpreted by these authors as pseudotachylytes that originated from low degrees of melting during past earthquakes.

[10] Sixteen thin sections were studied in this fault zone between 1110.37 and 1111.45 m depth in Hole A, including the destroyed hard black disk. We base most of our interpretations on descriptions from the core of the fault zone (Figure 2), and especially on one large thin section (2.1 × 8 cm) that encompasses the lower black gouge and the foliated sediments (Figure 3).

3.2. Black Gouge

[11] The black gouge is subdivided into several layers based on criteria such as isotropic texture, presence of cleavage or fractures, undeformed or deformed veins, compaction structures, grain size, percentage of clays, and orientation of clays. The cleavage intensity increases from the bottom to the top of the thin section, indicating an increasing apparent deformation from layer A to O.

3.2.1. Layer A: A 2 cm Thick Isotropic -Gouge

[12] At the base of the black gouge and above the broken black disk of hard material, the 2 cm thick gouge is characterized by an ultracataclastic texture with matrix-supported clasts. No brecciation, no large shear structures, no cleavage, and no banding can be observed in this fine-grained layer using an optical microscope (Figure 4a). Therefore, the gouge can be qualified as isotropic, except for a few thin clay-rich zones that will be described below. The isotropic gouge is a mixture of rounded fragments within an ultrafine light brown matrix (Figure 4a). The smallest fragments are monomineralic and mostly monocrystalline (quartz, feldspars, with small amounts of calcite, zircon, rutile, or tourmaline). Only 14 cracked quartz clasts, such as the one in Figure 4a (top middle) were counted on a 6 cm^2 surface. The largest quartz grains are 0.1 mm in diameter. A few polymineralic or polycrystalline clasts of calcite, chert, quartz-feldspar, or quartz-calcite aggregates have been observed. The largest (up to 0.9 mm) and more numerous polymineralic fragments are constituted by older dark brown gouges (Figure 4b). Except for two fragments which are identical to the material above the isotropic gouge layer, all of the large dark gouge fragments have similar textures as the broken hard black disk of ultracataclastic material

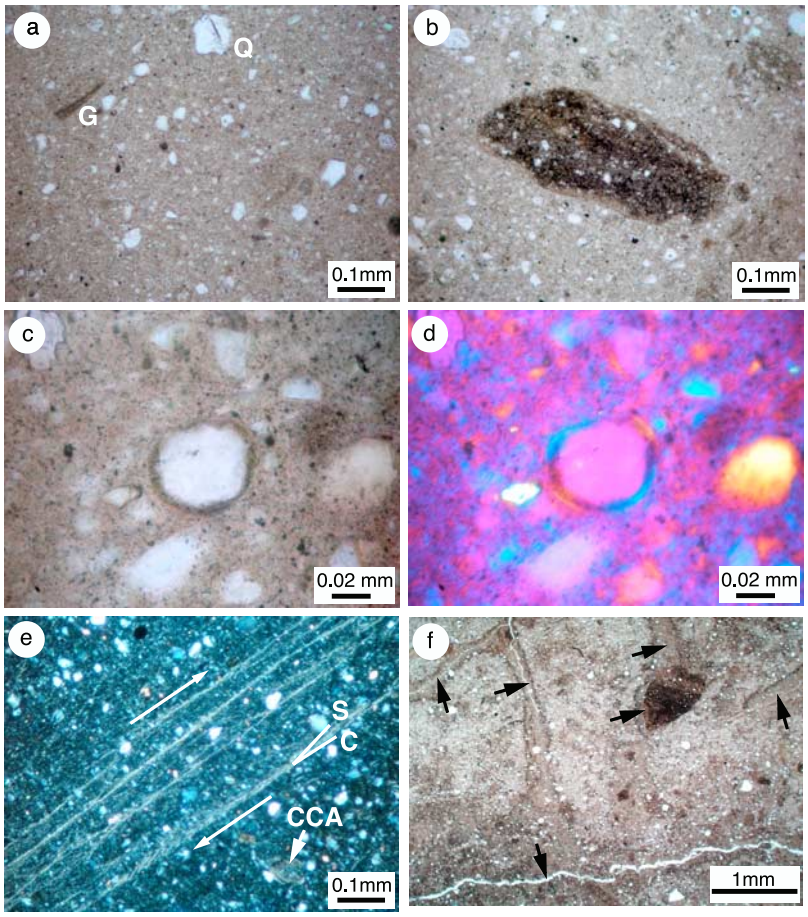

Figure 4. Microstructures in the isotropic gouge, layer A in Figure 3. All microphotographs are oriented as in Figure 3 except Figure 4e. (a) General aspect of the isotropic gouge showing the matrix-supported clasts which are either monomineralic, such as the fractured quartz fragment (Q), or fine-grained polymineralic gouge fragments (G). Plane polarized light. (b) Large dark gouge fragment within the isotropic fine-grained gouge. The fragment shows an internal cleavage. Plane polarized light. (c) Clay-clast aggregate (CCA) with a round quartz core and a brownish cortex made of clays. Plane polarized light. (d) Same as Figure 4c but under crossed polars with an additional gypsum plate (axis NE-SW). (e) Thin layers of fine-grained clays displaying a preferred orientation and a C-S structure indicating a top-to-the-right sense of shear (white arrows). The thin section has been slightly turned in order to place the clays at their maximum illumination, i.e., (001) at 45°. Note the CCA with a gouge fragment as a core at the bottom right. Crossed polars. (f) General view of the isotropic gouge showing the thin microfractures with their brownish haloes (black arrows). Note the rough geometry of the microfractures. Plane polarized light.

situated below the isotropic gouge layer. These gouge fragments display a peculiar mineralogical layering or a cleavage defined by preferentially oriented clays (Figures 4a, top left, and 4b). Most of the gouge fragments include finer-grained quartz clasts, as compared to the quartz clasts within the surrounding isotropic gouge (Figures 4a, 4b, and 4f). The large gouge fragments appear to be concentrated in the top third of the layer (Figure 5) and some are surrounded by an open crack now filled by epoxy (Figure 4f). One gouge fragment included within a larger gouge fragment has been observed, which may be explained by the fact that the lower hard black disk itself contains gouge fragments.

[13] Whatever their size, many monomineralic or gouge fragments display an obvious concentric clay coating, but this coating is particularly well defined around clasts smaller than 150 μm as a very fine-grained ($\ll$1 μm), brownish layer under plane polarized light (Figure 4c). The clays are illuminated in four sectors under crossed polars and display opposite blue or yellow colors under crossed polars plus a gypsum plate (Figure 4d), suggesting an orientation parallel to the clast margins. The position of yellow and blue sectors is consistent with the position of α and γ axes perpendicular and parallel to the (001) plane, respectively. The average thickness of the clay

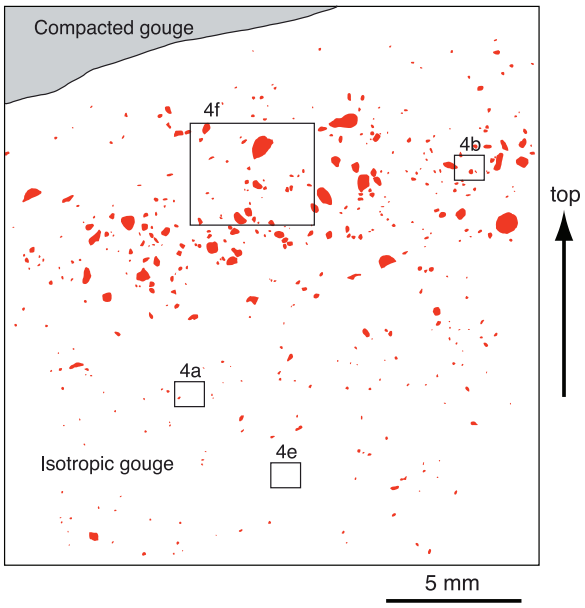

Figure 5. Grain size segregation of the gouge clasts in the isotropic gouge. Note that the largest clasts are within the upper top third of the gouge layer (proposed Brazil nut effect). Microphotographs of Figure 4 are shown by boxes.

cortex is 4.7 ± 2 μm (Figure 6a) and appears to be independent of the diameter of the central clast (Figure 6b). The variability of the cortex thickness may be related either to surface irregularities of the central clast or to the effect of oblique sections.

[14] Five very localized thin zones (Table 1) represent the only exceptions to the anisotropic texture of this gouge layer A. These zones are characterized by the alignment of clay particles (illite?) less than 10 μm in length. They are parallel to the fault plane, are observed on the entire width of the thin section, and are not disrupted within the gouge. The strongly preferred orientation of the clays at low angles to the fault or shear plane is suggested by the maximum illumination of the clays under crossed polars with a gypsum plate. Therefore, these thin zones have a typical C-S structure (Figure 4e) as defined by *Berthé et al.* [1979]. Following these authors and using the angle between the C and S planes and the thickness of each zone, we have roughly calculated a minimum 8.5 mm total displacement across the isotropic gouge (Table 1). These clay-rich zones have been locally reopened and filled either by epoxy or by calcite in one fracture in the lower part of the layer.

[15] The matrix of the isotropic gouge has a light beige color under the microscope, except around thin extensional fractures now filled by epoxy that show a 0.2 to 0.5 mm wide brown halo with a darker external rim (Figure 4f). These fractures are rough, intergranular, and go around the gouge fragments (Figure 4f). They are oriented either subparallel or subperpendicular to the fault plane on average and no apparent deformation is associated with them. The chemical composition of the gouge is homogeneous as shown by XRF elemental composition mapping (Figures 7a and 7b, bottom): no compositional layering is visible and Si, Ca, K, S, and Ti-rich spots simply correspond to monomineralic clasts of quartz, calcite, or plagioclase, K-feldspar, pyrite, or rutile, respectively. However, a very slight enrichment in Fe is clearly observed around late fractures (Figures 7a and 7b, bottom).

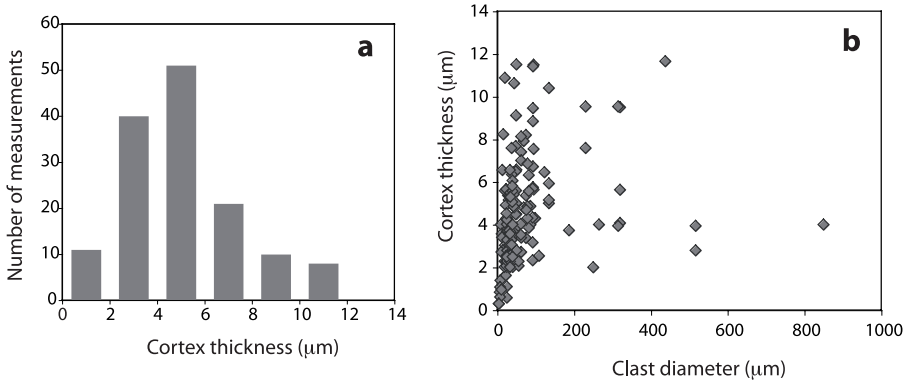

Figure 6. Characterization of the CCAs. Measurements of the clast diameter and the cortex thickness have been performed using microphotographs made with a petrographic microscope and a few SEM images. The accuracy of the measurements is on the order of ± 0.5 μm. (a) Histogram of the cortex thickness (mean 4.7 ± 2 μm). (b) Cortex thickness versus the largest dimension of the central clast. The cortex thickness is independent of the clast diameter for clasts larger than 150 μm.

Table 1. Small Clay-Rich Shear Zones Listed From Bottom to Top in the Isotropic Layer[a]

Zone/ Subzone	Thickness e, mm	Comments	Approx. C-S Angle α	Approx. Shear Angle γ[b]	Estimated Displacement d,[c] mm
A 1	0.05	high clay content, high LPO	3°	87°	0.95
A 2	0.45	medium clay content, C-S	5°	85°	5.10
B1	0.5	medium clay content, C-S	15°	47°	1.73
B2	0.025	high clay content, high LPO	6°	84°	0.23
C1	0.015	high clay content, high LPO	15°	74°	0.05
C2	0.002	high clay content, high LPO	15°	74°	0.01
C3	0.005	high clay content, high LPO	15°	74°	0.02
C4	0.002	high clay content, high LPO	15°	74°	0.01
D	0.2	medium clay content, C-S	30°	49°	0.23
E	0.3	medium clay content, C-S	40°	19°	0.11
				Total	8.44

[a] LPO is lattice preferred orientation. C-S is microstructures as described by *Berthé et al.* [1979].
[b] $\cot 2\alpha = 1/2 \tan \gamma$ et.
[c] $\tan \gamma = d/e$ [*Ramsay*, 1967].

3.2.2. Layers B to J: Compacted Gouges

[16] The boundary between the isotropic gouge layer and the upper compacted gouge layers is sharp, straight, and localized above the uppermost clay-rich C-S shear zone listed in Table 1. One major feature with high contrast relative to the isotropic layer consists of black irregular and curved fractures (Figure 8a) which are particularly abundant in layers B to F (Figure 3) but are also present in two gouge fragments in the isotropic gouge layer. These fractures are not associated with any peculiar optical feature under crossed polars (Figure 8b) and do not show any specific orientation relative to the fault plane. They do not correspond to a particular concentration of clays or black minerals but are air-filled and appear to be related to surface defects or topographic irregularities of the thin section.

[17] In contrast to the isotropic gouge, calcite veins are present in the deformed gouges (Figure 3 and Figures 8c, 8d, and 8f), although in a limited volume (<5% of the thin-section surface on average). They are generally thin (<20 μm wide) and display different degrees of strain. The undeformed calcite veins are restricted to a 3 mm thick zone (layers B to D in Figure 3) and appear as jigsaw patches (Figure 8c). Matching vein-wall irregularities indicate that they have a dilational origin (extension). Thin planar cracks at high angles to the fault plane (Figures 8d and 8f) display upward increasing apparent deformation by vertical shortening, as shown by folds (Figure 8d), mechanical twins, and rotation toward the fault plane. A very thin layering corresponding to a higher concentration of submicrometric black grains is present in the D and E layers (Figure 8e). This feature is accompanied by a fault-parallel cleavage defined by preferentially oriented clays (Figure 8f) or by very thin cracks defining conjugated sets relative to the fault plane and filled with crack-parallel oriented clays (Figure 8b). Chemical composition of these compacted gouge layers clearly shows compositional layering (Fe, Al, K, Mg, Si, and Ti) and carbonate veining (Figures 7b, top, and 7c), which are both absent in the isotropic gouge.

[18] The layers B to J of compacted gouges contain also many rounded clasts of older gouges. These are particularly abundant (nearly 30% areal extent) and large (up to 1 mm) in layers H and I (see Figure 3). An internal cleavage is observed in almost all of these clasts and is generally oblique to the fault-parallel cleavage of the surrounding matrix. This is particularly obvious on crossed polars with a gypsum plate. A few extensional localized shear bands are visible in layers B to F (see Figure 3). A fold deforming the H, I, and J layers, displays an axial planar cleavage oblique to the fault plane and is consistent with an upthrust movement (Figure 3). The upper black gouge of FZA1111 (Figure 2) displays similar microstructures to those of the B to J layers, i.e., rounded older gouge fragments and a fault-parallel cleavage.

3.3. Foliated Sediments

[19] As already stated above, the foliated sediments are located between two layers of black gouges

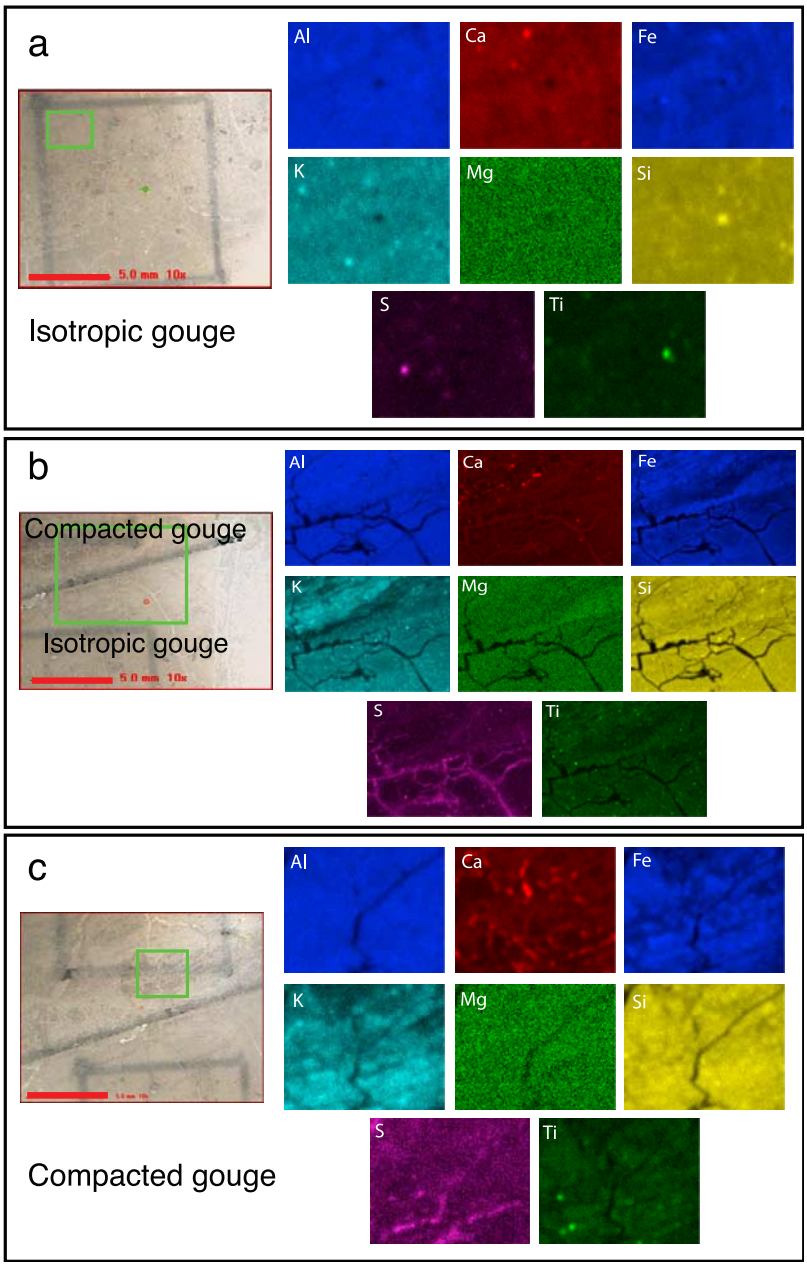

Figure 7. XRF element mapping of areas indicated by green boxes. The red bar on the photos on the left is 5 mm. Mg, because of its low Z, is less accurate than the other elements. The epoxy-filled cracks appear black for all elements except S. (a) Isotropic gouge. It is homogeneous except for some bright dots which are monomineralic fragments of calcite, K-feldspars, quartz, pyrite, or rutile. (b) The XRF map overlaps the limit (black line drawn on the back of the thin section) between the isotropic gouge on the bottom and the compacted gouge on the top. A compositional layering is visible in the compacted gouge, especially for Fe, K, Ti, and Mg. (c) Compacted gouge. As for zone B, the compositional layering is visible mostly for Fe, K, Si, and partly for S. A calcite vein and calcite patches appear on the Ca map.

(Figure 2) and are represented by the layers K to O on the thin section (Figure 3). They display a fault-parallel light to medium gray banding defined by the alternance of quartz-rich and clay-rich layers, respectively. Inherited sedimentary features can be recognized, such as fossils and detrital micas or chlorites.

[20] The major microstructural features of these layers is the larger average grain size compared to that of the gouges, with the diameters of quartz

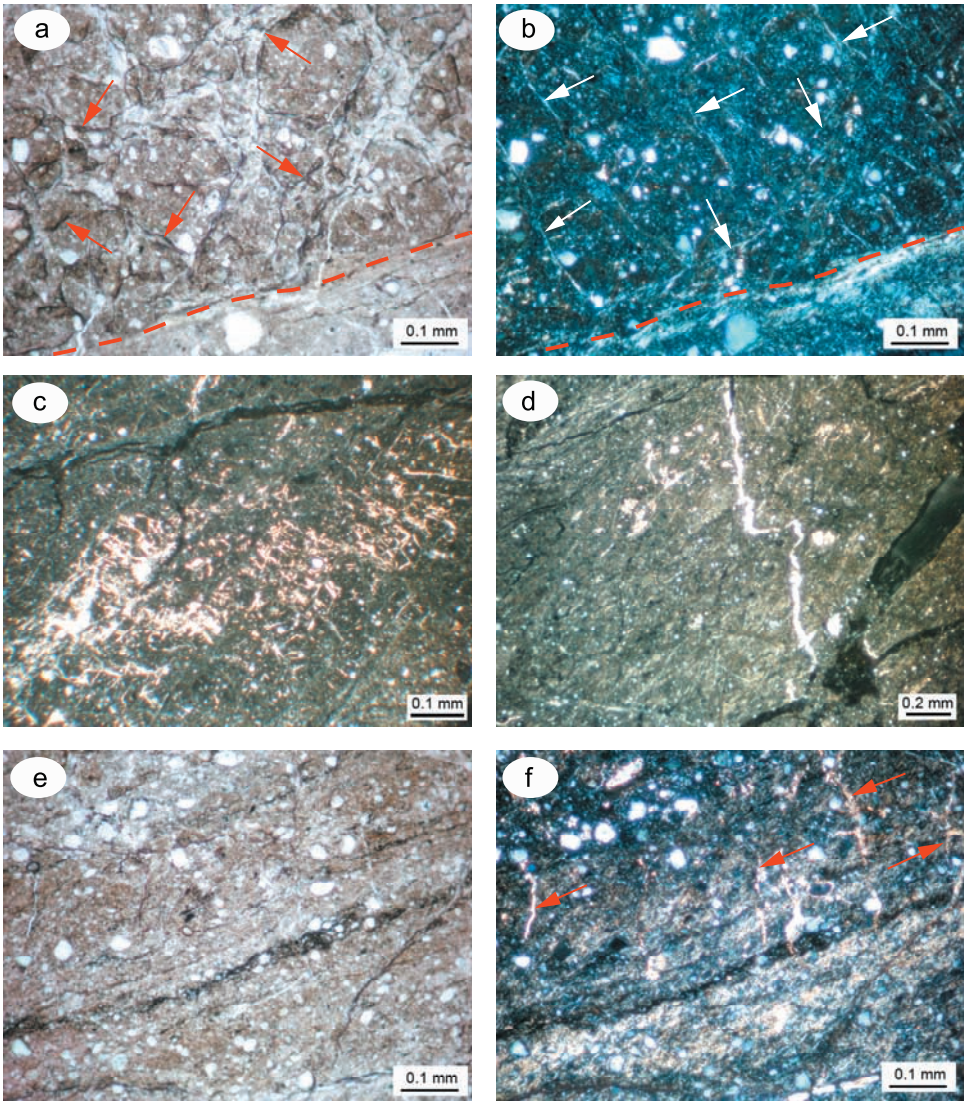

Figure 8. Microstructures in the compacted gouges. All microphotographs are oriented as in Figure 3. (a) Boundary (red broken line) between the isotropic gouge (lighter beige at the bottom) and the compacted gouge. Small black and irregular microfractures (red arrows) are restricted to the compacted gouge. Plane polarized light. (b) Same area as in Figure 8a but under crossed polars. The boundary between the isotropic gouge and the compacted gouge is characterized by a clay-rich layer (indicated by the red broken line and below). Note also the small clay-filled fractures (white arrows) in the compacted gouge which are either at a high or low angle to the boundary. (c) Dilational patch of calcite veins in the compacted gouge above the boundary with the isotropic gouge (layer D in Figure 3). Crossed polars. (d) Vertically shortened calcite vein (layer F in Figure 3). Crossed polars. (e) Thin compositional layering characterized by a high concentration of tiny black minerals. Plane polarized light. (f) Same area as Figure 8e under crossed polars. Note the high-angle calcite veins (red arrows) and the clay-rich layer showing a preferred orientation in the lower third of the microphotograph.

grains ranging up to 0.5 mm (Figures 9b and 9d). Although fracturing of these quartz grains appears to be ubiquitous, the fractured fragments are not scattered allowing for their virtual reassembly. Therefore, following the definition given by *Keulen et al.* [2007], they are not gouges but layers of cracked grains. The coarser-grained quartz-rich layers are permeated by calcite which is present as a cement in the pores, as filling material in grain-scale fractures, or as veins at high angles to the fault plane (Figures 9a and 9b). When present as a cement, calcite is clearly more abundant on the top of the sandstone layers than at their base. The calcite crystals within veins and cements are mechanically twinned and vertically shortened (Figures 9a and 9b), which is also the case for

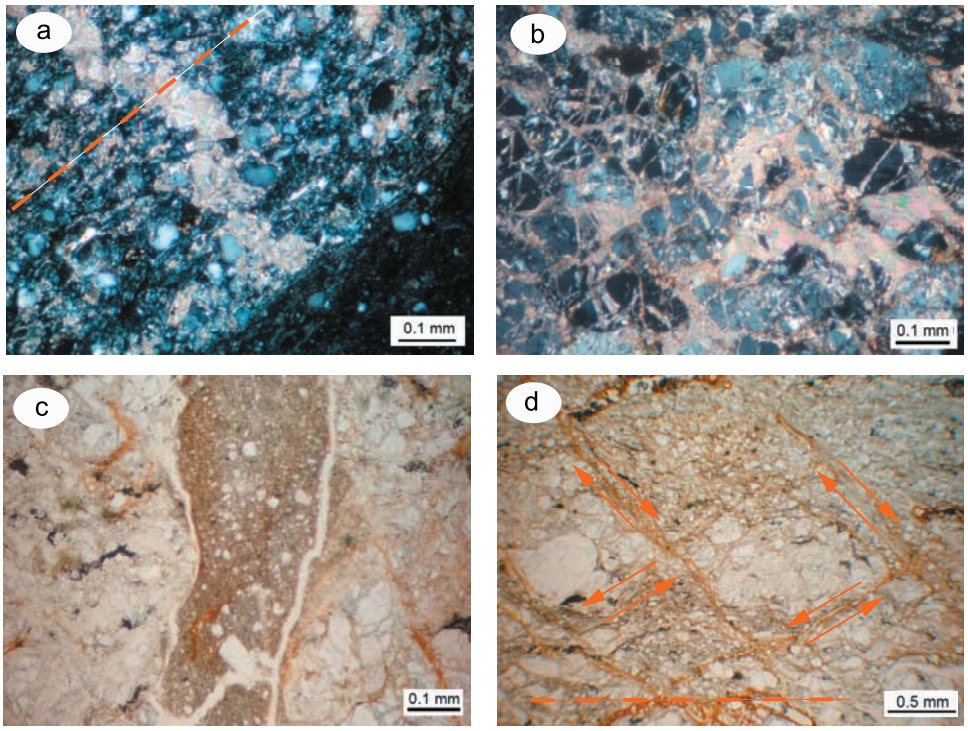

Figure 9. Microstructures in the deformed sediments. (a) Boundary between a quartz-rich (top) and a clay-rich (bottom right corner) layer (base of M on Figure 3). A calcite vein is vertically shortened and partly dissolved along the fault-parallel cleavage, indicated by a red broken line. Crossed polars. (b) Coarse-grained and quartz-rich layer showing subvertical transgranular fractures and intergranular pores filled by calcite. Crossed polars. (c) Fine-grained isotropic material injected in a fracture within deformed sandy sediments. Plane polarized light. (d) Deformed sediments showing variations in grain size and conjugated shears (red double arrows) symmetrical relative to the fault-parallel cleavage (red broken line). Plane polarized light.

detrital grains, micas, and clays which define a fault-parallel cleavage (Figures 9c and 9d). Conjugate shear bands in sandy layers are also indicative of a vertical shortening (Figure 9d). The sedimentary layering and cleavage are locally folded together (Figure 3, top of the thin section).

[21] In another thin section of these foliated sediments (NTU, TCDP3.1), we have observed narrow (<0.3 mm) fractures that have been injected by a fine-grained isotropic material (Figure 9c). Given the small size of the core sample, it was not possible to precisely determine the 3-D geometry of these fractures, but they are oriented at high angles to the fault plane and cleavage, are deformed at the boundary between quartz-rich and quartz-poor layers, and are sheared together with the surrounding foliated silty rocks (see Figure 2b).

3.4. FZB1136

[22] Sample FZB1136 from Hole B has already been the subject of an extensive, nondestructive characterization of its physical properties, such as density, porosity, magnetic susceptibility, natural gamma ray radiation and gamma ray attenuation [*Hirono et al.*, 2006b, 2007b], and X-ray computed tomography [*Hirono et al.*, 2008]. However, until now no detailed microstructural studies have been reported in the literature. We performed SEM observations on a complete 100 μm thick section across the FZB1136 fault zone in order to have information complementary to that given by the samples from FZA1111.

[23] The half core and the section assemblage are shown in Figure 10. The black gouge is localized in the 1136.26–1136.40 m interval between two gray gouges, an upper one (1136.22–1136.26 m) and a lower one (1136.40–1136.46 m) [*Hirono et al.*, 2007b, 2008]. This fault zone differs from FZA1111 by the absence of a black disk. Sedimentary features such as detrital micas, fossils, or delicate framboidal pyrites were observed above and below the two continuous white lines shown in Figure 10 and localized in sections 1 and 9.

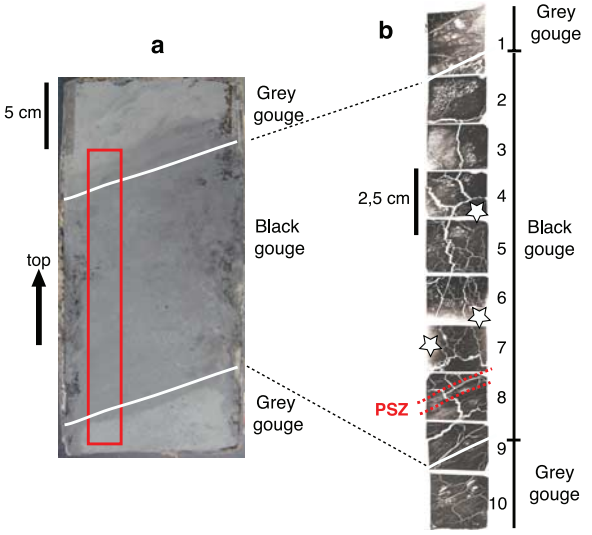

Figure 10. The FZB1136 fault zone. (a) Image of the core section FZB1136 and location of the 100 μm thick sections (rectangle). The black gouge is delimited by the two white lines and corresponds to the disappearance of sedimentary features. (b) Assembly of scans of the 100 μm thick sections 1 to 10 of the FZB1136 with the localization of the two white lines. The PSZ corresponds to the youngest gouge layer. White stars show CCAs localized in compacted gouge layers.

Therefore, the upper and lower gray gouges can be considered as deformed sediments and share similar deformation textures with the deformed sediments described in FZA1111, such as cleavage parallel to the fault plane, fractured grains and dilated sandy layers cemented by calcite, and thin shear zones.

[24] Between the two white lines, the black gouge exhibits a macroscopically homogeneous texture. However, thin section [*Hirono et al.*, 2008] and systematic SEM (this study) observations allow one to distinguish several layers of more or less compacted or deformed gouges displaying cleavage (sections 2 to 8), folds (section 2), small shear zones (all sections), calcite veins showing different degrees of strain (sections 3 to 6), and a probable gouge injection (section 6). Thus, the FZB1136 black gouge shares similar microstructures with the FZA1111 one. However, a 3 mm thick layer (Figure 10, between the broken red lines in section 8) is devoid of small shear zones, veins, or any later deformation structures. Its location corresponds to the low-density zone LZ2 described in X-ray computed tomographic images by *Hirono et al.* [2008]. Because of the absence of reworked or compacted microstructures (Figure 11a), this layer may be compared to the isotropic gouge layer in FZA1111. However, it is different because of its smaller thickness (0.3 cm versus 2 cm) and by its textural characteristics: it is a very fine grained ultracataclasite, is devoid of older gouge fragments at the scale of the section, and locally exhibits a layering defined by variations in concentrations of monomineralic clasts which are locally touching each other, or of very small clay minerals and tiny grains (Figure 11b). Very small heavy minerals (white on BSE-SEM images) present in this gouge were recognized as rutile, apatite, and undetermined Fe-S minerals.

[25] Interestingly, textures similar to those observed in FZA1111 isotropic gouge layer can be observed in compacted and sheared gouge layers, such as aggregates with a 5 to 10 μm thick clay cortex (white stars in Figure 10 and Figure 11c) or rounded gouge fragments (Figure 11d).

4. Discussion

[26] The FZA1111 and FZB1136 fault zones correspond with the surface rupture [*Ma*, 2005; *Hung et al.*, 2007; *Heermance et al.*, 2003], and with the slip zone identified in the northern shallow borehole [*Tanaka et al.*, 2006]. With respect to the surrounding country rock, the fault zones have a specific clay mineralogy [*Kuo et al.*, 2005; *Song et al.*, 2007], and are characterized by decreasing resistivity, lower density, Vp and Vs values, elevated Vp/Vs and Poisson's ratios, higher fracture density [*Hung et al.*, 2007], and frequent borehole breakouts [*Wu et al.*, 2007; *Lin et al.*, 2007]. Most importantly, temperature anomalies have been measured on this fault plane in the TCDP Hole A well [*Kano et al.*, 2006] as well as in other shallow boreholes [*Tanaka et al.*, 2006, 2007]. Therefore, these studies have already shown that the FZA1111 and the FZB1136 are the fault plane of the Chi-Chi earthquake.

4.1. Chi-Chi Earthquake Slip Zone

[27] In the FZA1111 and the FZB1136 samples, several layers of gouge have been distinguished which correspond to several past earthquakes, including Chi-Chi. Among these gouge layers, the 2 cm thick gouge at the bottom of the black gouge in FZA1111 is the only one to show a remarkable isotropic texture (the thin clay-rich zones excepted) and the absence of veins, fractures, or large shear zones suggesting that this layer has not been reworked by any subsequent slip event.

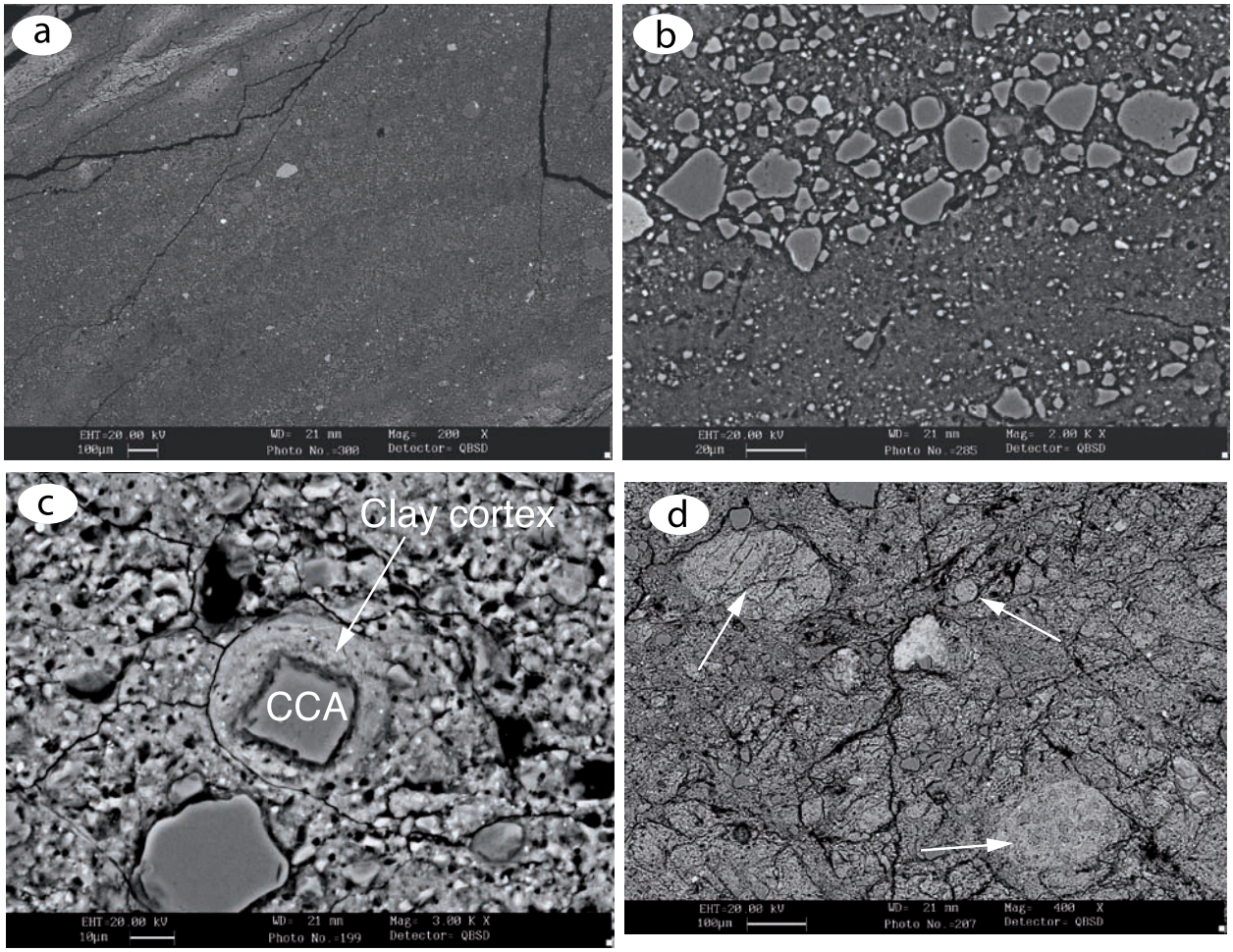

Figure 11. Backscattered electron SEM images of the FZB1136 black gouge. (a) Fine-grained PSZ in section 8. No shear-zones have been observed in this layer, which is thought to be the youngest gouge layer. Scale bar is 100 μm. (b) Detail of the layer shown in Figure 11a. Note the layering defined by heterogeneous grain size distribution. The upper layer contains large quartz clasts, whereas the lower one is very fine-grained and clay-rich. Scale bar is 20 μm. (c) CCA in section 6 (Figure 10). Note the fine-grained and dense 10 μm-thick clay-rich cortex around the central quartz clast. Scale bar is 10 μm. (d) Compacted gouge in section 4 (Figure 10) containing numerous rounded gouge fragments (white arrows). Scale bar is 100 μm.

This indicates that this isotropic gouge is the youngest PSZ of the Chelungpu fault and, consequently, is the Chi-Chi PSZ [*Kuo et al.*, 2005; *Ma et al.*, 2006]. All of the structural features described in the previous section suggest that the isotropic gouge results from a complete mixing of fragments of sedimentary grains, older calcite veins, or previous gouge layers originating mostly from the hard black material below the PSZ. The average grain size is lower than in the foliated sediments, which suggests that some fracturing or comminution processes have occurred. The quasi-absence of cracked fragments within FZA1111 indicates, however, that no stress concentration related to grain-to-grain contacts, i.e., no force chains, has existed in the isotropic gouge as it is structured now. This means that crushing or comminution was restricted to an early stage of the fault history or to an early stage of slip during the Chi-Chi earthquake.

[28] Until now, the only undisputed textural evidence for seismic faulting was the presence of pseudotachylytes [*Cowan*, 1999]. Some pseudotachylyte fragments have been found in the shallow drill hole that penetrates the southern part of the Chelungpu fault [*Otsuki et al.*, 2005]. Amorphous textures (vesicles and hourglass structures) have been described in two black disks in Hole B (FZB1194 and FZB1243) [*Hirono et al.*, 2006a]. *Kuo et al.* [2005] have mentioned similar textures

in the FZA1111 isotropic gouge layer but could not determine if these were localized in the gouge matrix or in some of the older gouge fragments plucked from the lower black disk and if they correspond to a quenched melt or to a gel similar to that produced by *di Toro et al.* [2004] during rotary-shear experiments. Consequently, pseudotachylytes produced by frictional melting during the Chi-Chi earthquake cannot be unambiguously demonstrated in the northern part of the Chelungpu fault.

[29] An important characteristic of the FZA1111 isotropic gouge is the presence of aggregates among the matrix-supported fragments. These natural microstructural features have been already found at the base of large landslides [*Beutner and Gerbi*, 2005] and within the gouge of the Alpine fault in New Zealand [*Warr and Cox*, 2001]. For the first time, they have been experimentally reproduced by *Boutareaud et al.* [2008a] from high-velocity rotary shear tests using a natural smectite-rich gouge as a starting material; they are termed clay-clast aggregates (CCAs hereafter) by these authors. CCAs observed in the FZA1111 isotropic gouge display a thinner clay cortex (5 μm versus 15 μm) than those experimentally produced. This difference may be simply related to the larger total displacement of the rotary shear experiments (30 to 55 m) compared to the slip during the Chi-Chi earthquake (approximately 5 m on the TCDP site) [*Yu et al.*, 2001]. As shown by *Boutareaud et al.* [2008b], the presence of smectite clay minerals in the gouge used in the experiments appears to be a key parameter for the formation of the CCAs because the amount of interlayer water that can be released while heating is very large [*Ferrage et al.*, 2005; *Michot et al.*, 2005]. This is also an important characteristic of the FZA1111 isotropic gouge, where smectites are almost the only clays present, with a minor occurrence of illite [*Kuo et al.*, 2005]. *Boutareaud* [2007] and *Boutareaud et al.* [2008a] have conducted rotary shear experiments at 0.09, 0.9, and 1.3 m/s. On the basis of temperature measurements during the experiments, the authors have modeled the thermal evolution in the gouge at 0.6 MPa normal stress and have shown that CCAs are only formed when frictional heating occurring in the gouge was sufficient to reach water vaporization (160°C at 0.6 MPa) during the early stage of slip, regardless of the water content of the initial gouge. These authors suggest that CCAs could be a new useful textural indicator of large slip at coseismic velocity with thermal pressurization [*Boutareaud et al.*, 2008a]. Therefore, the observation of CCAs in the FZA1111 isotropic gouge may imply that thermal pressurization occurred in the Chi-Chi earthquake slip zone, on at least the northern part of the fault where slip reached about 9 m [*Yu et al.*, 2001].

[30] CCA formation implies aggregation of clay particles around a central rolling clast, a process which is thought to be enhanced by surface tension phenomena or electrostatic forces in a thermally pressurized and fluidized clay-rich gouge [*Boutareaud et al.*, 2008a]. Consequently, CCAs indicate that complex processes should have controlled the behavior of very small sized particles in the gouge. If crushing and comminution were effective during the first stage of slip and contributed to decrease the overall grain size, fine particle aggregation around clasts may have modified the grain size distribution in the FZA1111 gouge. Consequently, the fracture energy released by the Chi-Chi earthquake [*Ma et al.*, 2006] may not be simply related to grain size distribution in the gouge and may point to some other mechanochemical processes that should also be considered in the energy budget of the Chi-Chi earthquake.

[31] The gouge fragments originating from the lower black disk are concentrated in the top third of the layer (Figure 5). Such a grain size segregation may be explained by two mechanisms. First, it may be compared to flotation of large blocks on top of viscous debris flows. However, we do not observe any flow texture in the gouge. Second, and we favor this interpretation, the observed grain size segregation of the gouge fragments perhaps obeys the Brazil nut effect (BNE), a phenomenon observed when an homogeneously distributed mixture of large and small nuts or beads is vertically shaken in a container, such that large particles migrate toward the top of the container. The BNE size segregation results from the competition between downward percolation of the small particles between the larger ones and buoyancy, which tends to push the heavier particles toward the bottom of the container [*Ciamarra et al.*, 2006; *Schröter et al.*, 2006]. Experimental BNE simulations have been conducted under air pressure, i.e., in a very low viscosity medium with upward flow of larger particles depending on the size and density ratios of the particles, their surface frictional properties, the total height of the layer, and the acceleration of the vibrations. Depending on these conditions, BNE segregation may or may not occur [*Ciamarra et al.*, 2006; *Schröter et al.*, 2006]. A high diameter ratio with almost no density contrast is favorable for BNE segregation, and this is the case of the

FZA1111 PSZ gouge where clasts are similar in composition but are of very different sizes. The total height of the layer (20 mm) is much larger than the largest particles (0.9 mm), and this configuration is also favorable to BNE size segregation [*Schröter et al.*, 2006]. The Chi-Chi peak ground acceleration reached 0.5 g at the surface of the hanging wall [*Chang et al.*, 2004], but acceleration on the fault plane at depth may have been larger than 10 g [*McGarr et al.*, 1981] which is within the range of shaking accelerations during experimental BNE grain size segregation (1 to 20 g range) [*Schröter et al.*, 2006]. The unknown parameters are the relative viscosity of the matrix and the friction coefficient of the fragments in FZA1111 PSZ. While the size segregation experiments are generally conducted in an air-filled container, the aging of particles (i.e., increasing friction coefficient) is a favorable condition for BNE size segregation [*Ulrich et al.*, 2007]. Gouge fragments may be considered to have high static friction properties. The observation that their size distribution obeys BNE shows that they were able to move and geometrically rearrange themselves in a very low viscosity medium during this particular seismic shaking event. Therefore, in addition to the presence of CCAs indicators for large seismic slip and thermal pressurization, the observed grain size segregation of gouge fragments strongly suggests that the gouge was fluidized during the Chi-Chi earthquake.

[32] In FZB1136, the inferred PSZ of the Chi-Chi earthquake has different textural characteristics than the FZA1111 isotropic gouge. First, it is much thinner (0.3 cm versus 2 cm) and second, it does not contain CCAs, but clay-rich foliated gouges alternating with clast-rich layers similar to foliated gouge described by *Boutareaud et al.* [2008a] in their high velocity rotary shear experiments. The existence of loaded grain contacts between quartz clasts suggests that fragmentation was still effective in the corresponding layers and that friction was still high [*Mair et al.*, 2002]. According to *Boutareaud et al.* [2008a], the foliated gouges is where heat is first produced by strain localization, which is then diffused through the whole gouge leading to thermal pressurization. As Holes A and B are 40 m apart in the downdip direction, such differences in FZA1111 and FZB1136 indicate that the Chi-Chi PSZ has variable thickness and structural signature and that physical and dynamic seismic processes may vary somewhat along the fault. Heat may have been produced by friction in the thin FZB1136 PSZ, while thermal pressurization inducing fluidization of the gouge may have been dominantly expressed in the thicker FZA1111 PSZ. However, thicker compacted gouge layers containing CCAs and gouge fragments are also observed in FZB1136 (Figures 11c and 11d), whereas thinner compacted but layered gouge layers are observed in FZA1111 (Figure 3 and Figures 4e and 4f). This means that textural signatures of physical and dynamic seismic processes may change in space along the fault plane and in time from one earthquake to another.

[33] As described in the previous sections, the only observed compositional layering in FZA1111 corresponds to thin clay-rich C-S layers that are indicative of low shear strain (approximately 8 mm of minimal displacement; Table 1). Because the isotropic gouge is interpreted as the Chi-Chi earthquake PSZ and these shear zones are not disrupted within the gouge, they are interpreted to have developed after the fluidization of the PSZ gouge and to be related to ductile deformation during the Chi-Chi postseismic shear. *Yu et al.* [2003] measured postseismic deformation using GPS data during 15 months after the Chi-Chi earthquake, which shows a spatial correlation between the smallest postseismic displacements and the largest coseismic displacements. At their AF25 station which is the closest one to the TCDP drill site, the measured horizontal displacement was approximately 48 mm after 15 months. Thus, the 8 mm estimate of ductile postseismic shear localized within the 2 cm thick slip zone is consistent with the GPS measurements. The very low postseismic deformation of the isotropic gouge also suggests that fluidization of the gouge was effective until the seismic slip stopped, due probably to the low permeability of the fault walls preventing the efficient escape of fluids.

[34] The precise age of the thin rough fractures with a brown halo which are present in the isotropic gouge is unknown. They are expected to be younger than the Chi-Chi earthquake and may be simply related to an artifact induced by drilling or by thin section preparation. The core samples were preserved in a cold chamber with a controlled humidity before sample distribution. Moreover, we can be confident that the cores did not dry out and that no iron-rich fluid percolated through the samples during stockage. Barium was not detected in the gouge based on XRF, indicating that these fractures were not contaminated by drilling mud. Whatever their age, these microfractures were the locus of Fe-rich fluid circulation leading to

iron enrichment in the wall rocks (Figures 7a and 7b). Their rough geometry indicates that they may have propagated at a subcritical rate [*Atkinson*, 1987]. They may be related to a rapidly distributed volume change in the isotropic gouge (C. Rowe, personal communication, 2008) after the Chi-Chi earthquake. Measured in situ hydraulic diffusivity by injection tests [*Doan et al.*, 2006] shows that the permeability values of the fault zone are high compared to the permeability of the host rocks measured by *Sone et al.* [2007b]. If these microfractures were formed in the isotropic gouge at depth after Chi-Chi, but before drilling, they could explain these high permeabilities. Nonetheless, the real age and origin of these fractures still remain a matter of debate.

4.2. Compacted Gouge: Interseismic Deformation of Previous Slip Zones

[35] Small irregular black cracks, compositional layering, and calcite veins are the most striking differences between the compacted gouge and the isotropic gouge layer below. As the small cracks do not correspond to any compositional variation and do not show any specific orientation, it is not possible to interpret them as dissolution features, such as stylolites for example. As they appear to be air-filled and correlated with topographic defects on the surface of the thin section, they can be considered to be artifacts related to the thin section preparation. Nevertheless, these artifacts do not exist in the isotropic gouge matrix and are indicative of a discrepancy in the physical properties of the compacted gouges compared to the isotropic gouge, i.e., possessing higher strength potentially due to a greater degree of compaction.

[36] Evidence for dissolution is found in the thin compositional layering described in the D-E layers, defined by a higher concentration in small black grains or clay minerals, and corresponding to higher concentrations of Fe, Al, K, Mg, Si, and Ti (Figures 7b and 7c). This is particularly evident for Fe and Ti in the thin black layers and for K and Mg where the concentration of clays is higher. This fine-scale compositional layering is interpreted as the result of a passive concentration of insoluble minerals in a plane normal to the maximum stress induced by the dissolution of soluble minerals [*Durney*, 1976; *Gratier*, 1987]. This process may also have accentuated a previously existing layering similar to that of the foliated gouge described in FZB1136 PSZ. Such a pressure solution mechanism may have contributed to the compaction of the gouge layers above layer A, increasing their strength and decreasing their permeability.

[37] Calcite veins within the compacted gouges provide information on fluid circulation at different stages of the fault zone evolution. Just above the isotropic gouge, 3-D dilational patches of undeformed calcite veins indicate that these veins are recent and related to hydraulic fracturing. We suggest that they are induced by coseismic fluid redistribution from the isotropic gouge below and have been induced by the Chi-Chi earthquake. The contrasting composition of calcite-rich fault walls and calcite-poor gouge in the FZB1136 has been interpreted by *Hirono et al.* [2007a] as resulting from the thermal decomposition of carbonates at temperatures higher than 850°C during seismic slip, as has been experimentally reproduced by *Han et al.* [2007]. However, clays, and especially smectites, are able to produce a large quantity of water by dehydration between 200 and 385°C, depending on the interlayer cations [*Wu et al.*, 1997b; *Michot et al.*, 2005]. Moreover, *Brantut et al.* [2008] have observed an analogous large release of water during high-velocity rotary shear experiments using clay-rich gouges as starting material. We suggest that an important release of water from clays, and especially smectites, by frictional heating during seismic slip could have diluted the pore water within the isotropic gouge and thus enhanced calcite dissolutional removal in the gouge. Moreover, higher temperatures would lead to faster carbonate dissolution kinetics. Subsequent coseismic fluid redistribution within the hanging wall may then have locally induced hydraulic fracturing of the hanging wall, leading to precipitation of calcite.

[38] On the basis of the isotopic signature of calcite veins around the fault zone, *Wang et al.* [2005] have shown that the fluids were a mixture of meteoritic and seawater with a very limited distance of circulation due to a relatively low hydraulic diffusivity and that the vein-filling carbonates originated from dissolution of the numerous microfossils observed in the surrounding sediments. Following the reasoning of these authors, we estimate that the Chelungpu fault does not represent an important fluid conduit connected to greater depths. This assumption is consistent with the observed limited volume of calcite veins in a restricted volume of wall rock compared to what has been described in the Nojima fault, where carbonate veins related to coseismic fluid redistri-

bution are observed several meters away from the fault [*Boullier et al.*, 2004a].

[39] Deformation of the calcite veins (layers C to H, Figure 3) and folds with an axial planar cleavage (layer H, Figure 3) are indicative of a shortening perpendicular to the fault plane, which also probably results from a pressure solution process [*Durney*, 1976; *Rutter*, 1976; *Gratier*, 1987; *Le Guen et al.*, 2007]. This process implies a succession in space and time of three mechanisms, (1) dissolution at loci of stress concentration, (2) diffusion of solute within a trapped intergranular fluid film, and (3) crystallization at minimum stress boundaries. This process is kinetically controlled by the slowest mechanism, which is diffusion [*Rutter*, 1976]. In addition, this process implies a stress lower than the strength of the material in combination with a low strain rate. Therefore, it is assumed to be operative during postseismic to interseismic intervals [*Gratier and Gamond*, 1990]. As apparent finite deformation of the compacted gouge layers increases from the bottom to the top, as indicated by increased shortening of the calcite veins, it is suggested that the age of the gouge layers in FZA1111 is correspondingly older from the bottom to the top, as each layer has registered more interseismic strain than the layer immediately below.

[40] Apart from the compaction microstructures, the compacted gouges in FZA1111 and FZB1136 share similar textures with the isotropic gouge layer. Indeed they contain no cracked quartz but instead contain matrix-supported clasts, CCAs, and numerous gouge fragments. These similarities suggest that the compacted gouges constitute ancient slip zones representative of past earthquakes similar to Chi-Chi with regards to their seismological characteristics (slip, magnitude, slip weakening mechanisms. . .). It is not easy to count the totality of these seismic events because we could not observe a continuous section across the whole gouge zone. However, on the basis of nine determined gouge layers (A to I in Figure 3), the two hard black disk materials themselves containing gouge fragments, and the observation of gouge fragments in the compacted gouge layers (B to I in Figure 3), we suggest that the observed gouge section could correspond to 15 to 20 major earthquakes. We could not observe the whole upper black gouge in FZA1111, and thus we do not know how many seismic events have been registered there. The total displacement on the FZA1111 has been determined to be 0.3 km and attributed to approximately 35 Chi-Chi-equivalent earthquakes by *Yue et al.* [2005]. Our observations are consistent with these estimates.

4.3. Foliated Sediments: Seismic and Aseismic Deformation

[41] We previously stated that the very fine grained material injected within fractures in the foliated sediments is similar to the isotropic gouge matrix of the FZA1111 PSZ. *Otsuki et al.* [2005] and *Ujiie* [2005] describe similar clay-rich injections in the northern shallow borehole through the Chelungpu fault. Following *Lin* [1996], *Rowe et al.* [2005], and *Ujiie et al.* [2007], we interpret these features as coseismic injections of fluidized gouge originating from a lower-level gouge layer. The jigsaw lines of fine-grained black material observed in the upper light gray clay-rich gouge (Figure 2) are probably also deformed gouge injections originating from the upper black gouge layer. All the gouge injections observed in FZA1111 are deformed and sheared together with the surrounding foliated sediments in a way similar to the compacted gouge, i.e., by the low strain rate pressure solution mechanism [*Durney*, 1976; *Rutter*, 1976; *Gratier*, 1987; *Le Guen et al.*, 2007]. By comparison with what has been described in the Nojima fault zone [*Boullier et al.*, 2004b], this pressure solution mechanism is interpreted as acting mostly during interseismic stages. Therefore, like the compacted gouges, the gouge injections should correspond to past earthquakes.

[42] Because of the small size of the core sample, we did not observe undeformed gouge injections originating from the FZA1111 isotropic gouge layer that could be related to the Chi-Chi earthquake, but it is not excluded that such injections may also have occurred elsewhere and not just at the drill hole. Indeed, all of the textural characteristics of the isotropic gouge (very fine grain size, matrix-supported clasts, no loaded grain contacts, presence of CCAs, and occurrence of Brazil nut segregation indicating thermal pressurization and low viscosity of the gouge matrix) are consistent with its fluidization required for its mobilization and injection in the above surrounding fault rocks [*Ujiie et al.*, 2007].

[43] Three-dimensional dilation of the top of sandy layers below and above the FZA1111 black gouge and their impregnation by calcite are indicative of hydraulic fracturing induced by high fluid pressure. The clay-rich layers may have acted as impermeable caps allowing compartmentalization of the sediments and formation of small-size cells of high fluid pressure within sandy layers. By analogy with

the seismic valve model proposed by *Sibson et al.* [1988], it is tentatively suggested that this high fluid pressure occurred during the preseismic stage, before the interconnection of the high pressure cells induced by the seismic rupture [*Sibson*, 1994]. Deformation of the calcite cement probably occurred therafter by twinning and pressure solution during the interseismic stage.

4.4. Slip-Weakening Processes in the Chi-Chi Slip Zone

[44] The Chi-Chi earthquake is characterized by a contrast in seismological behavior of the northern and southern areas of the fault. *Ma et al.* [2003] have proposed the elastohydrodynamic lubrication mechanism for the northern part, following the model presented by *Brodsky and Kanamori* [2001]. In this model lubrication pressure increases during slip within the viscous PSZ gouge layer and contributes to decreasing the frictional stress by elastically deforming the asperities and widening the fault wall distance. Similar internal pressure in the gouge may result from thermal pressurization when frictional heating induces a pore fluid pressure increase [*Sibson*, 1973; *Lachenbruch*, 1980; *Wibberley and Shimamoto*, 2003, 2005], if fluid is trapped within the gouge pores. Such a mechanism has been proposed for the Chi-Chi PSZ by *Tanaka et al.* [2006, 2007] and *Kano et al.* [2006] on the basis of temperature anomalies measured in the shallow boreholes and in TCDP hole A, respectively. According to *Boutareaud et al.* [2008a], CCAs constitute reliable evidence of frictional heating and thermal pressurization and formed during experiments when the temperature reached the water vapor phase boundary at 160°C. In FZA1111 PSZ, pore pressure before slip was less than 26 MPa (lithostatic gradient) and higher than 11.1 MPa (hydrostatic gradient), with a present-day temperature of 46.5°C [*Kano et al.*, 2006]. A minimum 300–400°C increase in temperature would be necessary to bring the pore water into the vapor or critical state in the 11 to 26 MPa pressure range [*Roedder and Bodnar*, 1980]. There is no direct evidence that the isotropic gouge of the Chi-Chi earthquake was heated to such elevated temperatures, although temperature measurements in boreholes across the Chi-Chi PSZ have shown temperature increases 1 [*Tanaka et al.*, 2007] and 6 years [*Kano et al.*, 2006] after the earthquake. However, 400°C temperature increases have been registered by magnetic minerals in the black disks from FZB1194 and FZB1243 [*Mishima et al.*, 2006], as well as by vitrinite reflectance in a very narrow fault zone from the southern shallow drill hole [*Sakaguchi et al.*, 2007]. Therefore, as past earthquakes on the Chelungpu fault have produced such frictional heat, we would expect the occurrence of similar processes during the Chi-Chi earthquake within the isotropic gouge.

[45] A numerical simulation based on the calculation proposed by *Wibberley and Shimamoto* [2005] and on measurements of physical transport properties of the FZA1111 fault zone [*Sone*, 2006; *Sone et al.*, 2007b] has been performed to evaluate the consequences of frictional heating of FZA1111 in terms of thermal pressurization and a slip-weakening effect (see Appendix A). The simulation confirms that all of the conditions were met for thermal pressurization in the 2 cm wide PSZ during the Chi-Chi earthquake.

[46] To conclude, microstructural analysis of the Chelungpu fault gouge from the two TCDP boreholes are consistent with fluidization and thermal pressurization of the Chi-Chi PSZ and therefore may explain the exceptionally large velocities and ground displacement observed in the northern part of the Chelungpu fault.

5. Conclusions

[47] On the basis of a detailed microscale description of samples from the TCDP project, we conclude the following:

[48] 1. We have recognized the Chi-Chi earthquake Principal Slip Zone in the fault zones FZA1111 and FZB1136 by the lack of any later deformation. In the FZA1111, the PSZ is a 2 cm thick isotropic gouge characterized by matrix supported clasts, the absence of loaded grain contacts between these clasts, the presence of clay clasts aggregates (CCAs), and older gouge fragments segregated on the top third of the slip zone according to the Brazil nut effect. In the FZB1136, it is a 0.3 cm thick, very fine grained zone displaying alternation of clay-rich and clast-rich layers. For the first time, CCAs are recognized as slip indicators in a recent slip zone in an important active fault.

[49] 2. By analogy with CCA-producing experiments performed by *Boutareaud et al.* [2008a], we suggest that pore water in the isotropic gouge reached the vapor or critical state and therefore was heated to 300–400°C at 1111m depth. Release of water from clays in the gouge by frictional heating may have increased the water content of

the gouge, contributing to an increase of the pore pressure.

[50] 3. All of the described structures suggest that the gouge was fluidized by thermal pressurization resulting from strain localization and heat production in places such as the thin PSZ in the FZB1136, this in itself inducing fluidization of the isotropic gouge that was concentrated on wider PSZ, such as FZA1111.

[51] 4. This work demonstrates that clays have a very important role for slip weakening processes and fluid-rock interactions in shallow, clay-rich slip zones.

[52] 5. Thin undeformed calcite veins within the compacted gouges above the PSZ in the FZA1111 are interpreted to be representative of the coseismic redistribution of fluids expelled from the PSZ and are thought to be related to the Chi-Chi earthquake. However, the quantity of precipitated carbonate is small (less than 5% in a thin section) and indicates that only small volumes of fluids were able to escape from the PSZ toward the low permeability fault walls.

[53] 6. Although low-rate deformation by pressure solution has partly modified their microstructural signature, several layers of compacted gouges in FZA1111 and FZB1136 may be recognized as the PSZ of past earthquakes having characteristics similar to the Chi-Chi event.

[54] On the basis of microscopic observations of the PSZ of the Chelungpu fault gouge, the conclusions of this work are of primary importance for mesoscopic and microscopic observations of retrieved fault gouges from coring programs conducted through active faults such as the Nankai subduction zone [*Park et al.*, 2002].

Appendix A: Thermal Pressurization of the Chi-Chi Slip Zone

[55] Here we present the results of a simple numerical simulation of thermal pressurization based on the calculation proposed by *Wibberley and Shimamoto* [2005] and *Boutareaud et al.* [2008c]. We consider a simple one-dimensional fluid and heat-flow model in the direction perpendicular to the fault. On the basis of microstructural observations of the isotropic gouge (i.e., this paper), we also consider that all of the fault displacement and related dynamic weakening processes are localized along a well-defined, laterally continuous and planar 2 cm thick (FZA1111) or 0.3 cm thick (FZB1136) gouge slip zone. Below we discuss the relevance of our results.

[56] As most of the mechanical frictional energy is converted into heat [*Scholz*, 2002], heat represents the major component of the energy budget of earthquakes. For that purpose, it constitutes a key physical parameter that controls the dynamics of the slip-weakening process (see *Rice* [2006] for a review). As two possible end-members, frictional heating of pore fluids can lead either to thermal expansion of the fluids, resulting in drainage out of the heated slip zone, or to pressurization of the fluids if trapped within pores [*Sibson*, 1973].

[57] A characteristic distance that controls the loss of fluid under pressure during the entire slip duration is the hydraulic diffusion length scale L_h [*Mase and Smith*, 1987; *Lachenbruch*, 1980; *Wibberley and Shimamoto*, 2005]:

$$L_h = (D_h \Psi)^{1/2} \tag{A1}$$

where D_h is the hydraulic diffusivity and Ψ a characteristic time controlling the rate of thermal pressurization. These two parameters can be defined as:

$$D_h = \frac{k}{\eta \beta_c}; \tag{A2}$$

$$\beta_c = (\beta_b - \beta_s) + \phi(\beta_f - \beta_s) \tag{A3}$$

$$\Psi = \frac{\rho c}{\mu_d \Gamma V}; \tag{A4}$$

$$\Gamma = \frac{\phi \alpha_w + (1-\phi)\alpha_m - \alpha_{sf}}{\beta_c} \tag{A5}$$

where k is the permeability function (see Table A1) determined by best fitting the data obtained from laboratory measurements on FZA1111 gouge samples by *Sone* [2006] and *Sone et al.* [2007b], β_c is the storage capacity, β_f is the compressibility of liquid water, β_s is the compressibility of individual grains, β_b is a function of the gouge bulk framework compressibility determined by best fitting the data obtained from laboratory measurements on the FZA1111 fault gouge by *Sone* [2006] and *Sone et al.* [2007b], ρ is the clay-rich fault gouge density, c is the clay-rich fault gouge specific heat capacity, μ_d is the dynamic coefficient of friction, Γ is the thermal pressuriza-

Table A1. Physical Parameters With Symbols, Values, and Units Used in the Thermal Pressurization Numerical Modeling

Property	Symbol	Value	Units
Permeability	k	–[a]	m^2
Porosity		–[a]	
Total slip zone width	$2W$	2×10^{-2}	m
		0.3×10^{-2}	m
Water dynamic viscosity	η	2.82×10^{-4}	Pa s^{b}
Storage capacity	β_c	–[a]	Pa^{-1b}
Compressibility of liquid water	β_f	4.3×10^{-10}	Pa^{-1b}
Compressibility of individual grains	β_s	1.2×10^{-11}	Pa^{-1b}
Water thermal expansivity	α_w	6×10^{-4}	K^{-1b}
Mineral thermal expansivity	α_m	2×10^{-5}	K^{-1b}
Gouge thermal expansivity	α_{sf}	1×10^{-5}	K^{-1b}
Gouge density	ρ	2000	kg m^{-3c}
Gouge specific heat capacity	c	1000	J kg^{-1} K^{-1c}
Dynamic friction coefficient	μ_d	0.4	
Relative slip velocity	V	2	m s^{-1}

[a] Values based on the logarithmic function to unloading data reported by *Sone et al.* [2007b]. The method is applied from *Boutareaud* [2007], with (1) the permeability values follow equations of the form: $k = k_0 \times \exp[-\gamma \times (P_e - P_0)]$, where k_0 is the permeability equal to 4×10^{-18} m^2 at a reference pressure $P_0 = 0$, and (2) the porosity values follow equations of the form $= {}_0 \times \exp[-\alpha \times (P_e - P_0)]$, where ${}_0$ is the porosity equal to 0.18 at a reference pressure $P_0 = 0$.

[b] Values assumed to be constant, based on *Lachenbruch* [1980], *Mase and Smith* [1987], *Wibberley and Shimamoto* [2005].

[c] Values based on data from *Tanaka et al.* [2007].

tion coefficient, V is the relative slip velocity, η is the fluid dynamic viscosity, α_w is the thermal expansivity of water, φ is the porosity function determined by best fitting the data obtained from laboratory measurements on the FZA1111 fault gouge by *Sone* [2006] and *Sone et al.* [2007b], α_m is the mineral thermal expansivity, and α_{sf} is the thermal expansivity of the porous medium (see Table A1).

[58] Considering a half-slip zone width W of 1 cm (e.g., PSZ in FZA1111) or 0.15 cm (e.g., PSZ in FZB1136), the calculated hydraulic diffusion length scale L_h is 0.01 cm and 0.03 cm, respectively. It can be shown that $L_h \ll W$, which implies that the amount of fluid loss from the slip zone during the fault slip duration can be assumed to be negligible. Thus, the numerical model assumes a trapped fluid.

[59] The rate of thermal pressurization is the difference between the rate of pore pressure buildup due to frictional heating and the rate of pressure dissipation due to fluid flow in the slipping zone. Assuming the entire frictional work is transformed into heat, the rate of frictional heating during faulting is equal to:

$$\frac{dT}{dt} = \frac{\frac{d\tau}{dt} \times V}{\rho \times c \times w} \tag{A6}$$

where τ is the fault frictional resistance. Assuming an effective stress for a constant slip rate, the frictional resistance τ of the fault is given by:

$$\frac{d\tau}{dt} = \mu_d \times \left(\sigma_n - \frac{dP}{dt}\right) \tag{A7}$$

Combining equations (6) and (7), it results:

$$\frac{dT}{dt} = \frac{\mu_d \times \left(\sigma_n - \frac{dP}{dt}\right) \times V}{\rho \times c \times w} \tag{A8}$$

Taking into account the absence of fluid loss (see above), the corresponding rate of undrained pore pressure buildup is:

$$\frac{dP_1}{dt} = \Gamma \times \frac{dT}{dt} = \Gamma \times \frac{\mu_d \times \left(\sigma_n - \frac{dP}{dt}\right) \times V}{\rho \times c \times w} \tag{A9}$$

Following classical solutions for heat diffusion as an analog for fluid pressure diffusion [*Carslaw and Jaeger*, 1959], the rate of fluid pressure dissipation in the center of the shear zone can be estimated as:

$$\frac{dP_2}{dt} = -D_h \times \frac{dP_1}{dt} \times \left(\frac{\pi}{2w}\right)^2 \times e^{-D_h \times \left(\frac{\pi}{2w}\right)^2 \times t} \tag{A10}$$

The rate of thermal pressurization Ω is the difference between the rate of pore pressure buildup due to frictional heating (equation (9)) and the rate of pressure dissipation due to fluid flow (equation (10)). Integration of the result with respect to time allows calculation of the fluid pressure evolution within the gouge slip zone. Finally, the frictional resistance Π of the fault through time (then through displacement) is given as follows:

$$\frac{d\Pi}{dt} = \mu_d \times \left(\frac{d\sigma_e}{dt}\right) \times V \tag{A11}$$

considering that the effective stress σ_e is the difference between constant normal stress σ_n at considered depth and rate of thermal pressurization Ω. Figure A1 shows the result of our analysis for the

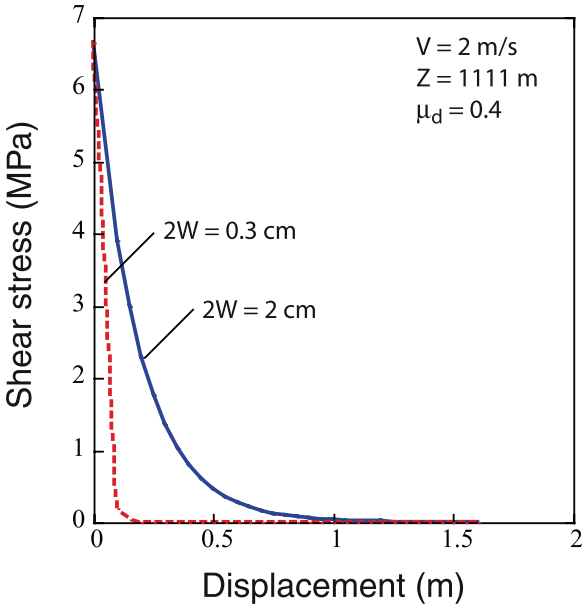

Figure A1. Results of modeling of the thermal pressurization process for the PSZ showing the effects of frictional heating during seismic slip at a 1111 m depth, 4 m/s slip velocity and for a 0.4 dynamic friction coefficient for a PSZ-thickness for 0.3 cm (red curve) and 2 cm (blue curve), respectively.

two gouge slip zones. It states that for an effective pressure P_e of 16.7 MPa, assuming a lithostatic pressure gradient of 25 MPa/km and a fluid pressure gradient of 10 MPa/km (at 1111 m depth), all of the necessary conditions are fulfilled for thermal pressurization to be effective for a slip weakening distance *Dc* of ~1 m on a 2 cm wide PSZ or of ~0.1 m on a 0.3 cm wide PSZ, with a total fault strength reduction of 6.7 MPa. The results also show that the gouge slip zone thickness is a key parameter that significantly affects the thermal pressurization process, with better efficiency for the thinner gouge thicknesses, which is consistent with the results obtained by *Noda and Shimamoto* [2005] from a more elaborate numerical analysis.

[60] These results have two important implications for the determination of the seismic process. First, the thermal pressurization process, which is supported by the presence of CCA microstructures and BNE segregation of underlying plucked gouge fragments, appears to be efficient in the two gouge zones at 1111 m depth. Second, the calculated slip weakening distance D_c, which is of the same order of magnitude as those determined from seismological studies ranging from 0.05 to about 1 m [*Ide and Takeo*, 1997; *Mikumo et al.*, 2003], occurs over timescales of the order of one second and appears to be representative of the typical risetime and stress drop of large earthquakes. The combination of these two results provides important evidence that tend to validate a possible occurrence of thermal pressurization during the Chi-Chi earthquake. However, our two D_c values are a factor of 10 lower than the D_c estimated by *Ma et al.* [2006] for the Chi-Chi earthquake (nearly 5 m) at the northern end of the fault, and our numerical simulation overestimates by about 2 MPa the coseismic fault strength reduction estimated by *Ma et al.* [2006]. On the basis of the fact that our numerical analysis does not take into account the slip rate change that accompanies the fault slip with a peak velocity that occurred at few seconds after the slip initiation [*Ma et al.*, 2003], one reason explaining this discrepancy in both D_c and $\Delta\tau$ may be related to the type of slip weakening mechanism that was operative. Indeed, the physical conditions responsible for the parameters of a specific weakening mechanism would primarily depend on the rate of frictional heating during the initial stages of slip [*Bizzarri and Cocco*, 2006; *Sulem et al.*, 2007; *Boutareaud*, 2007]. We can also consider an isovolumetric shear at constant shear strain rate in our model. This results in several physical parameters being constant (such as the storage capacity or the water compressibility among others); however, this does not agree with the microstructural evidence that suggests a gouge water phase transition. To the best of our knowledge, few studies account for the phase transition from liquid to water vapor induced by frictional heating of both water expelled from clay interlayers and the gouge pore water [*Sulem et al.*, 2007; *Mizoguchi et al.*, 2007; *Boutareaud et al.*, 2008a]. These results point out that the properties of water during the rapid phase transition, properties that depend on pressure and temperature (in addition to the amount of CO_2 dissolved in water), should be seriously taken into account for future thermal pressurization process calculations.

Acknowledgments

[61] The authors are very grateful to Michel Bouchon for encouragements and scientific stimulations and to Hiroki Sone for giving us his laboratory measurements conducted on FZA1111 gouge samples. We would like also to thank Thibault Candela, Fabrice Cotton, Mai-Linh Doan, Bruno Lanson, Olivier Vidal, and Christopher Wibberley for fruitful discussions concerning different aspects of this paper. Particular thanks go to Li-Wei Kuo and Yu-Min Chu for their help in this program. Very constructive comments made by the reviewers (T. F. Wong, C. Rowe, and an anonymous reviewer) and the editor J. Tarduno helped improve the content and clarity of the manuscript. Olivier Romeyer (Chambéry), Frédéric Charlot (Grenoble), and Lin Hsu (Hualien) are thanked for their

technical assistance during SEM work and Christophe Nevado (Geosciences Montpellier) for making thin sections on the difficult FZB1136 gouge material. Roland Hellmann has kindly checked the language. This work has been funded by NSC to SRS (grants 93-2119-M-002 −028 and 94-2119-M-002-022), by the French Ministry of Foreign Affairs (PAI ORCHID 2006), by ANR (Programme Catastrophes Telluriques et Tsunamis, ACTS Taiwan, ANR-06-CATT-001-01), and by International Laboratory CNRS-NSC France-Taiwan ADEPT. AMB, ECY, and SRS are also affiliated with the France/Taiwan International Associated Laboratory ADEPT (CNRS, NSC).

References

Atkinson, B. K. (1987), Introduction to fracture mechanics and its geophysical applications, in *Fracture Mechanics of Rocks*, edited by B. K. Atkinson, pp. 1–26, Academic, London.

Berthé, D., P. Choukroune, and P. Jégouzo (1979), Orthogneiss, mylonite and non coaxial deformation of granites: The example of the South American Shear Zone, *J. Struct. Geol.*, *1*, 31–42, doi:10.1016/0191-8141(79)90019-1.

Beutner, E. C., and G. P. Gerbi (2005), Catastrophic emplacement of the Heart Mountain block slide, Wyoming and Montana, USA, *Geol. Soc. Am. Bull.*, *117*, 724–735, doi:10.1130/B25451.1.

Bizzarri, A., and M. Cocco (2006), A thermal pressurization model for the spontaneous dynamic rupture propagation on a three-dimensional fault: 1. Methodological approach, *J. Geophys. Res.*, *111*, B05303, doi:10.1029/2005JB003862.

Boullier, A.-M., K. Fujimoto, T. Ohtani, G. Roman-Ross, E. Lewin, H. Ito, P. Pezard, and B. Ildefonse (2004a), Textural evidence for recent co-seismic circulation of fluids in the Nojima fault zone, Awaji island, Japan, *Tectonophysics*, *378*, 165–181, doi:10.1016/j.tecto.2003.09.006.

Boullier, A. M., K. Fujimoto, H. Ito, T. Ohtani, N. Keulen, O. Fabbri, D. Amitrano, M. Dubois, and P. Pezard (2004b), Structural evolution of the Nojima fault (Awaji Island, Japan) revisited from the GSJ drill hole at Hirabayashi, *Earth Planets Space*, *56*(12), 1233–1240.

Boutareaud, S. (2007), Slip-weakening mechanisms at high slip-velocities: Insights from analogue and numerical modellings, Ph.D. thesis, Univ. de Franche-Comté, Besançon, France.

Boutareaud, S., D.-G. Calugaru, R. Han, O. Fabbri, K. Mizoguchi, A. Tsutsumi, and T. Shimamoto (2008a), Clay-clast agregates: A new structural evidence for seismic sliding?, *Geophys. Res. Lett.*, *35*, L05302, doi:10.1029/2007GL032554.

Boutareaud, S., A. M. Boullier, P. Beck, D.-G. Calugaru, R. Han, and A. Tsutsumi (2008b), Clast-clay agregates as new indicator of shallow crustal seismic slips, *Geophys. Res. Abstr.*, *10*, Abstract EGU2008-A-04694.

Boutareaud, S., C. A. J. Wibberley, O. Fabbri, and T. Shimamoto (2008c), Permeability structure and co-seismic thermal pressurization on fault branches: Insights from the Usukidani Fault, Japan, in *The Internal Structure of Fault Zones: Mechanical and Fluid Flow Properties*, edited by C. A. J. Wibberley et al., *Geol. Soc. London Spec. Publ.*, *299*, 341–361.

Brantut, N., A. Schubnel, J. Rouzaud, F. Brunet, and T. Shimamoto (2008), High velocity frictional properties of a clay-bearing fault gouge and implications for earthquake mechanics, *J. Geophys. Res.*, *113*, B10401, doi:10.1029/2007JB005551.

Brodsky, E., and H. Kanamori (2001), Elastohydrodynamic lubrication of faults, *J. Geophys. Res.*, *106*(B8), 16,357–16,374, doi:10.1029/2001JB000430.

Carslaw, H. S., and J. C. Jaeger (1959), *Conduction of Heat in Solids*, 510 pp., Oxford Univ. Press, Oxford, U.K.

Chai, H. T. (1972), Structure and tectonic evolution of Taiwan, *Am. J. Sci.*, *272*, 389–422.

Chang, T. Y., F. Cotton, Y. B. Tsai, and J. Angelier (2004), Quantification of hanging wall effects on ground motion: Some insights from the 1999 Chi-Chi earthquake, *Bull. Seismol. Soc. Am.*, *94*(6), 2186–2197, doi:10.1785/0120030233.

Chen, K. C., B. S. Huang, J. H. Wang, W. G. Huang, T. M. Chang, R. D. Hwang, H. C. Chiu, and C. C. P. Tsai (2001b), An observation of rupture pulses of the 20 September 1999 Chi-Chi, Taiwan, earthquake from near-field seismograms, *Bull. Seismol. Soc. Am.*, *91*(5), 1247–1254, doi:10.1785/0120000716.

Chen, Y. G., W. S. Chen, J. C. Lee, Y. H. Lee, C. T. Lee, H. C. Chang, and C. H. Lo (2001a), Surface rupture of 1999 Chi-Chi earthquake yield insights on active tectonics of central Taiwan, *Bull. Seismol. Soc. Am.*, *91*(5), 977–985, doi:10.1785/0120000721.

Ciamarra, M. P., M. D. De Vizia, A. Fierro, M. Tarzia, A. Coniglio, and N. Nicodemi (2006), Granular species segregation under vertical tapping: Effects of size, density, friction, and shaking amplitude, *Phys. Rev. Lett.*, *96*, 058001, doi:10.1103/PhysRevLett.96.058001.

Cornet, F. H., P. Bernard, and I. Moretti (2004), The Corinth Rift Laboratory, *C. R. Geosci.*, *336*(4–5), 235–241, doi:10.1016/j.crte.2004.02.001.

Cowan, D. S. (1999), Do faults preserve a record of seismic slip? A field geologist's opinion, *J. Struct. Geol.*, *21*, 995–1001, doi:10.1016/S0191-8141(99)00046-2.

di Toro, G., D. L. Goldsby, and T. E. Tullis (2004), Friction falls toward zero in quartz rock as slip velocity approaches seismic rates, *Nature*, *427*, 436–439, doi:10.1038/nature02249.

Doan, M. L., E. E. Brodsky, Y. Kano, and K. F. Ma (2006), In situ measurement of the hydraulic diffusivity of the active Chelungpu fault, Taiwan, *Geophys. Res. Lett.*, *33*, L16317, doi:10.1029/2006GL026889.

Durney, D. W. (1976), Pressure solution and crystallization deformation, *Philos. Trans. R. Soc. London, Ser. A*, *283*, 229–240, doi:10.1098/rsta.1976.0081.

Ferrage, E., B. Lanson, B. A. Sakharov, and V. A. Drits (2005), Investigation on smectite hydration properties by modelling experimental X-ray diffraction patterns: Part I. Montmorillonite hydration properties, *Am. Mineral.*, *90*, 1358–1374, doi:10.2138/am.2005.1776.

Gratier, J. P. (1987), Pressure solution-deposition creep and associated tectonic differentiation in sedimentary rocks, in *Deformation in Sediments and Sedimentary Rocks*, edited by M. E. Jones and R. M. F. Preston, *Geol. Soc. London Spec. Publ.*, *29*, 25–38.

Gratier, J. P., and J. F. Gamond (1990), Transition between seismic and aseismic deformation in the upper crust, in *Deformation Mechanisms, Rheology and Tectonics*, edited by R. J. Knipe and E. H. Rutter, *Geol. Soc. London Spec. Publ.*, *54*, 461–473.

Han, R., T. Shimamoto, T. Hirose, J. H. Ree, and J. I. Ando (2007), Ultralow friction of carbonate faults caused by thermal decomposition, *Science*, *316*, 878–881, doi:10.1126/science.1139763.

Heermance, R., Z. K. Shipton, and J. P. Evans (2003), Fault structure control on fault slip and ground motion during the 1999 rupture of the Chelungpu fault, Taiwan, *Bull. Seismol. Soc. Am.*, *93*(3), 1034–1050, doi:10.1785/0120010230.

Hickman, S., M. D. Zoback, and W. E. Ellsworth (2004), Introduction to special section: Preparing for the San Andreas Fault Observatory at Depth, *Geophys. Res. Lett.*, *31*, L12S01, doi:10.1029/2004GL020688.

Hirono, T., et al. (2006a), Evidence of frictional melting from disk-shaped black material, discovered within the Taiwan Chelungpu fault system, *Geophys. Res. Lett.*, *33*, L19311, doi:10.1029/2006GL027329.

Hirono, T., et al. (2006b), High magnetic susceptibility of fault gouge within Taiwan Chelungpu fault: Nondestructive continuous measurements of physical and chemical properties in fault rocks recovered from Hole B, TCDP, *Geophys. Res. Lett.*, *33*, L15303, doi:10.1029/2006GL026133.

Hirono, T., et al. (2007a), A chemical kinetic approach to estimate dynamic shear stress during the 1999 Taiwan Chi-Chi earthquake, *Geophys. Res. Lett.*, *34*, L19308, doi:10.1029/2007GL030743.

Hirono, T., et al. (2007b), Non-destructive continuous physical property measurements of core samples recovered from Hole B, Taiwan Chelungpu-fault Drilling Project, *J. Geophys. Res.*, *112*, B07404, doi:10.1029/2006JB004738.

Hirono, H., et al. (2008), Characterization of slip zone associated with the 1999 Taiwan Chi-Chi earthquake: X-ray CT image analyses and microstructural observations of the Taiwan Chelungpu fault, *Tectonophysics*, *449*, 63–84, doi:10.1016/j.tecto.2007.12.002.

Ho, C. S. (1986), A synthesis of the geologic evolution of Taiwan, *Tectonophysics*, *125*, 1–16, doi:10.1016/0040-1951(86)90004-1.

Ho, C. S. (1988), *An Introduction to the Geology of Taiwan—Explanatory Text of the Geologic Map of Taiwan*, 163 pp., Cent. Geol. Surv., Taipei, Taiwan.

Hung, J. H., Y. H. Wu, E. C. Yeh, J. C. Wu, and and the TCDP Scientific Party (2007), Subsurface structure, physical properties, and fault zone characteristics in the scientific drill holes of Taiwan Chelungpu-fault Drilling Project, *Terr. Atmos. Ocean. Sci.*, *18*(2), 271–293, doi:10.3319/TAO.2007.18.2.271(TCDP).

Ide, S., and M. Takeo (1997), Determination of constitutive relations of fault slip based on seismic wave analysis, *J. Geophys. Res.*, *102*, 27,379–27,391, doi:10.1029/97JB02675.

Kano, Y., J. Mori, R. Fujio, H. Ito, T. Yanagidani, S. Nakao, and K.-F. Ma (2006), Heat signature on the Chelungpu fault associated with the 1999 Chi-Chi, Taiwan earthquake, *Geophys. Res. Lett.*, *33*, L14306, doi:10.1029/2006GL026733.

Kao, H., and W. P. Chen (2000), The Chi-Chi earthquake sequence: Active out-of-sequence thrust faulting in Taiwan, *Science*, *288*, 2346–2349, doi:10.1126/science.288.5475.2346.

Keulen, N., R. Heilbronner, H. Stünitz, A. M. Boullier, and H. Ito (2007), Grain size distributions of fault rocks: A comparison between experimentally and naturally deformed granitoids, *J. Struct. Geol.*, *29*, 1282–1300, doi:10.1016/j.jsg.2007.04.003.

Kuo, L. W., S. R. Song, and H. Y. Chen (2005), Characteristics of clay mineralogy in the fault zone of the TCDP and its implication, *Eos Trans. AGU*, *86*(52), Fall Meet. Suppl., Abstract T43D–05.

Lachenbruch, A. H. (1980), Frictional heating, fluid pressure, and the resistance to fault motion, *J. Geophys. Res.*, *85*(B11), 6097–6112, doi:10.1029/JB085iB11p06097.

Lallemand, S., Y. Font, H. Bijwaard, and H. Kao (2001), New insights on 3-D plates interaction near Taiwan from tomography and tectonic implications, *Tectonophysics*, *335*(3–4), 229–253, doi:10.1016/S0040-1951(01)00071-3.

Le Guen, Y., F. Renard, R. Hellmann, E. Brosse, M. Collombet, D. Tisserand, and J.-P. Gratier (2007), Enhanced deformation of limestone and sandstone in the presence of high pCO2 fluids, *J. Geophys. Res.*, *112*, B05421, doi:10.1029/2006JB004637.

Lin, A. (1996), Injection veins of crushing-originated pseudotachylyte and fault gouge during seismic faulting, *Eng. Geol. Amsterdam*, *43*(2–3), 213–224, doi:10.1016/0013-7952(96)00062-2.

Lin, W., E. C. Yeh, H. Ito, J. H. Hung, T. Hirono, W. Soh, K. F. Ma, M. Kinoshita, C. Y. Wang, and S. R. Song (2007), Current stress state and principal stress rotations in the vicinity of the Chelungpu fault induced by the 1999 Chi-Chi, Taiwan, earthquake, *Geophys. Res. Lett.*, *34*, L16307, doi:10.1029/2007GL030515.

Ma, K. F. (2005), Slip zone and energetic of a large earthquake from seismological modeling and fault core of TCDP, *Eos Trans. AGU*, *86*(52), Fall Meet. Suppl., Abstract T43D–02.

Ma, K. F., J. Mori, S. J. Lee, and S. B. Yu (2001), Spatial and temporal distribution of slip for the 1999 Chi-Chi, Taiwan earthquake, *Bull. Seismol. Soc. Am.*, *91*(5), 1069–1087, doi:10.1785/0120000728.

Ma, K. F., E. E. Brodsky, J. Mori, C. Ji, T. R. A. Song, and H. Kanamori (2003), Evidence for fault lubrication during the 1999 Chi-Chi, Taiwan, earthquake (Mw7.6), *Geophys. Res. Lett.*, *30*(5), 1244, doi:10.1029/2002GL015380.

Ma, K. F., et al. (2006), Slip zone and energetics of a large earthquake from the Taiwan Chelungpu-fault Drilling Project, *Nature*, *444*, 473–476, doi:10.1038/nature05253.

Mair, K., K. M. Frye, and C. Marone (2002), Influence of grain characteristics on the friction of granular shear zones, *J. Geophys. Res.*, *107*(B10), 2219, doi:10.1029/2001JB000516.

Mase, C. W., and L. Smith (1987), Effects of frictional heating on the thermal, hydrologic and mechanical response of a fault, *J. Geophys. Res.*, *92*(B7), 6249–6272, doi:10.1029/JB092iB07p06249.

McGarr, A., R. W. E. Green, and S. M. Spottiswoode (1981), Strong ground motion of mine tremors: Some implications for near-source ground motion parameters, *Bull. Seismol. Soc. Am.*, *71*, 295–319.

Michot, L. J., I. Bihannic, M. Pelletier, E. Rinnert, and J. L. Robert (2005), Hydration and swelling of synthetic Na-saponites: Influence of layer charge, *Am. Mineral.*, *90*, 166–172, doi:10.2138/am.2005.1600.

Mikumo, T., K. B. Olsen, E. Fukuyama, and Y. Yag (2003), Stress-breakdown time and slip-weakening distance inferred from slip-velocity functions on earthquake faults, *Bull. Seismol. Soc. Am.*, *93*(1), 264–282, doi:10.1785/0120020082.

Mishima, T., T. Hirono, W. Soh, M. Ikehara, W. Lin, W. Tanikawa, E. C. Yeh, S. R. Song, and C. Wang (2006), Thermal history estimation of the Taiwan Chelungpu fault using rock-magnetic methods, *Geophys. Res. Lett.*, *33*, L23311, doi:10.1029/2006GL028088.

Mizoguchi, K., M. Takahashi, K. Masuda, and E. Fukuyama (2007), Fault strength drop due to phase transitions in the pore fluid, *Geophys. Res. Lett.*, *34*, L09313, doi:10.1029/2007GL029345.

Noda, X., and T. Shimamoto (2005), Thermal pressurization and slip-weakening distance of a fault: An example of the Hanaore fault, *Bull. Seismol. Soc. Am.*, *95*, 1224–1233, doi:10.1785/0120040089.

Ohtani, T., K. Fujimoto, H. Ito, H. Tanaka, N. Tomida, and T. Higuchi (2000), Fault rocks and paleo- to recent fluid characteristics from the bore-hole survey of the Nojima fault

rupture in the 1995 Kobe earthquake, southwest Japan, *J. Geophys. Res.*, *105*(B7), 16161–16171, doi:10.1029/2000JB900086.

Otsuki, K., T. Uduki, N. Monzawa, and H. Tanaka (2005), Clayey injection veins and pseudotachylyte from two boreholes penetrating the Chelungpu fault, Taiwan: Their implications for the contrastive seismic slip behaviors during the 1999 Chi-Chi earthquake, *Isl. Arc*, *14*, 22–36, doi:10.1111/j.1440-1738.2004.00455.x.

Park, J. O., T. Tsuru, S. Kodaira, P. R. Cummins, and Y. Kaneda (2002), Splay fault branching along the Nankai subduction zone, *Science*, *297*(5584), 1157–1160, doi:10.1126/science.1074111.

Pathier, E., B. Fruneau, B. Deffontaines, J. Angelier, C. P. Chang, S. B. Yu, and C. T. Lee (2003), Co-seismic displacements of the footwall of the Chelungpu fault by the 1999 Taiwan, Chi-Chi earthquake from InSAR and GPS data, *Earth Planet. Sci. Lett.*, *212*, 73–88, doi:10.1016/S0012-821X(03)00244-9.

Ramsay, J. G. (1967), *Folding and Fracturing of Rocks*, 568 pp., Blackburn, Caldwell, N. J.

Rice, J. R. (2006), Heating and weakening of faults during earthquake slip, *J. Geophys. Res.*, *111*, B05311, doi:10.1029/2005JB004006.

Roedder, E., and R. J. Bodnar (1980), Geologic pressure determinations from fluid inclusion studies, *Annu. Rev. Earth Planet. Sci.*, *8*, 263–301, doi:10.1146/annurev.ea.08.050180.001403.

Rowe, C. D., J. C. Moore, F. Meneghini, and A. W. McKeirnan (2005), Large-scale pseudotachylytes and fluidized cataclasites from an ancient subduction thrust fault, *Geology*, *33*(12), 937–940, doi:10.1130/G21856.1.

Rutter, E. (1976), The kinetics of rock deformation by pressure solution, *Philos. Trans. R. Soc. London, Ser. A*, *283*, 203–219, doi:10.1098/rsta.1976.0079.

Sakaguchi, A., A. Yanagihara, K. Ujiie, H. Tanaka, and M. Kameyama (2007), Thermal maturity of a fold–thrust belt based on vitrinite reflectance analysis in the Western Foothills complex, western Taiwan, *Tectonophysics*, *443*, 220–232, doi:10.1016/j.tecto.2007.01.017.

Scholz, C. H. (2002), *The Mechanics of Earthquakes and Faulting*, 471 pp., Cambridge Univ. Press, Cambridge, U. K.

Schröter, M., S. Ulrich, J. Kreft, J. B. Swift, and H. L. Swinney (2006), Mechanisms in the size segregation of a binary granular mixture, *Phys. Rev. E*, *74*, 011307, doi:10.1103/PhysRevE.74.011307.

Sibson, R. H. (1973), Interactions between temperature and pore-pressure during earthquake faulting: A mechanism for spatial or total stress relief, *Nat. Phys. Sci.*, *243*, 66–68.

Sibson, R. H. (1994), Crustal stress, faulting and fluid flow, in *Geofluids: Origin, Migration, and Evolution of Fluids in Sedimentary Basins*, edited by J. Parnell, *Geol. Soc. London Spec. Publ.*, *78*, 69–84.

Sibson, R. H. (2003), Thickness of the seismic slip zone, *Bull. Seismol. Soc. Am.*, *93*(3), 1169–1178, doi:10.1785/0120020061.

Sibson, R. H., F. Robert, and K. H. Poulsen (1988), High angle reverse fault, fluid-pressure cycling and mesothermal gold quartz deposits, *Geology*, *16*, 551–555, doi:10.1130/0091-7613(1988)016<0551:HARFFP>2.3.CO;2.

Sone, H. (2006), Structural description of cores from the Taiwan Chelungpu-fault Drilling Project and the fault weakening process inferred from frictional and transport properties of fault zone core samples, 101 pp., Master's thesis, Kyoto Univ., Kyoto, Japan.

Sone, H., E. C. Yeh, T. Nakaya, J. H. Hung, K. F. Ma, C. Y. Wang, S. R. Song, and T. Shimamoto (2007a), Mesoscopic structural observations of cores from the Chelungpu fault system, Taiwan Chelungpu-fault Drilling Project Hole-A, Taiwan, *Terr. Atmos. Ocean. Sci.*, *18*(2), 359–377, doi:10.3319/TAO.2007.18.2.359(TCDP).

Sone, H., H. Noda, and T. Shimamoto (2007b), The co-seismic fault weakening processes inferred from frictional and transport properties of fault rocks, TCDP, *Sci. Drill.*, *1*, 97, doi:10.2204/iodp.sd.s01.06.2007.

Song, S. R., L. W. Kuo, E. C. Yeh, C. Y. Wang, J. H. Hung, and K. F. Ma (2007), Characteristics of the lithology, fault-related rocks and fault zone structures in TCDP Hole-A, *Terr. Atmos. Ocean. Sci.*, *18*(2), 243–269, doi:10.3319/TAO.2007.18.2.243(TCDP).

Sulem, J., P. Lazar, and I. Vardoulakis (2007), Thermo-poro-mechanical properties of clayey gouge and application to rapid fault shearing, *Int. J. Numer. Anal. Methods Geomech.*, *31*, 523–540, doi:10.1002/nag.584.

Tanaka, H., K. Fujimoto, T. Ohtani, and H. Ito (2001), Structural and chemical characterization of shear zones in the freshly activated Nojima fault, Awaji Island, southwest Japan, *J. Geophys. Res.*, *106*(B5), 8789–8810, doi:10.1029/2000JB900444.

Tanaka, H., W. C. Chen, C. Y. Wang, K. F. Ma, N. Urata, J. Mori, and M. Ando (2006), Frictional heat from faulting of the 1999 Chi-Chi, Taiwan earthquake, *Geophys. Res. Lett.*, *33*, L16316, doi:10.1029/2006GL026673.

Tanaka, H., W. M. Chen, K. Kawabata, and N. Urata (2007), Thermal properties across the Chelungpu fault zone and evaluations of positive thermal anomaly on the slip zones: Are these residuals of heat from faulting?, *Geophys. Res. Lett.*, *34*, L01309, doi:10.1029/2006GL028153.

Teng, L. S. (1990), Geotectonic evolution of late Cenozoic arc-continent collision in Taiwan, *Tectonophysics*, *183*, 57–76, doi:10.1016/0040-1951(90)90188-E.

Ujiie, K. (2005), Fault rock analysis of the northern part of the Chelungpu fault and its relation to earthquake faulting of the 1999 Chi-Chi earthquake, Taiwan, *Isl. Arc*, *14*, 2–11, doi:10.1111/j.1440-1738.2004.00453.x.

Ujiie, K., A. Yamaguchi, G. Kimura, and S. Toh (2007), Fluidization of granular material in a subduction thrust at seismogenic depths, *Earth Planet. Sci. Lett.*, *259*, 307–318, doi:10.1016/j.epsl.2007.04.049.

Ulrich, S., M. Schröter, and H. L. Swinney (2007), Influence of friction on granular segregation, *Phys. Rev. E*, *76*, 042301, doi:10.1103/PhysRevE.76.042301.

Wang, C. Y., C. H. Chang, and H. Y. Yen (2000), An interpretation of the 1999 Chi-Chi earthquake in Taiwan based on the thin-skinned thrust model, *Terr. Atmos. Ocean. Sci.*, *11*, 609–630.

Wang, P. L., J. Wu, L. H. Lin, E. C. Yeh, Y. G. Chen, and S. R. Song (2005), Isotopic evidence of fluid processes in fault-related rocks from TCDP drill cores in Taiwan, *Eos Trans. AGU*, *86*(52), Fall Meet. Suppl., Abstract T51A–1313.

Warr, L. N., and S. J. Cox (2001), Clay mineral transformations and weakening mechanisms along the Alpine fault, New Zealand, in *The Nature and Significance of Fault Zone Weakening*, edited by R. E. Holdsworth et al., *Geol. Soc. London Spec. Publ.*, *78*, 85–101.

Wibberley, C. A. J., and T. Shimamoto (2003), Internal structure and permeability of major strike-slip fault-zones: The Median Tectonic Line in Mie prefecture, Southwest Japan, *J. Struct. Geol.*, *25*, 59–78, doi:10.1016/S0191-8141(02)00014-7.

Wibberley, C. A. J., and T. Shimamoto (2005), Earthquake slip weakening and asperities explained by thermal pressurization, *Nature*, *436*, 689–692, doi:10.1038/nature03901.

Wu, F. T., R. J. Rau, and D. Salzberg (1997a), Taiwan orogeny: Thin-skinned or lithospheric collision?, *Tectonophysics*, *274*, 191–220, doi:10.1016/S0040-1951(96)00304-6.

Wu, H.-Y., K.-F. Ma, M. Zoback, N. Boness, H. Ito, J.-H. Hung, and S. Hickman (2007), Stress orientations of Taiwan Chelungpu-fault Drilling Project (TCDP) Hole-A as observed from geophysical logs, *Geophys. Res. Lett.*, *34*, L01303, doi:10.1029/2006GL028050.

Wu, T. C., W. A. Bassett, W. L. Huang, S. Guggenheim, and A. F. Koster van Gross (1997b), Montmorillonite under high H_2O pressures: Stability of hydrate phases, rehydration hysteresis, and the effect of interlayer cations, *Am. Mineral.*, *82*, 69–78.

Yeh, E. C., et al. (2007), Core description and characteristics of fault zones from Hola-A of the Taiwan Chelungpu-fault Drlling Project, *Terr. Atmos. Ocean. Sci.*, *18*(2), 327–357, doi:10.3319/TAO.2007.18.2.327(TCDP).

Yu, S. B., et al. (2001), Preseismic deformation and co-seismic displacement associated with the 1999 Chi-Chi, Taiwan, earthquake, *Bull. Seismol. Soc. Am.*, *91*, 995–1012, doi:10.1785/0120000722.

Yu, S. B., Y. J. Hsu, L. C. Kuo, H. Y. Chen, and C. C. Liu (2003), GPS measurement of post-seismic deformation following the 1999 Chi-Chi, Taiwan, earthquake, *J. Geophys. Res.*, *108*(B11), 2520, doi:10.1029/2003JB002396.

Yue, L. F., J. Suppe, and J. H. Hung (2005), Structural geology of a classic thrust belt earthquake: The 1999 Chi-Chi earthquake Taiwan (Mw7.6), *J. Struct. Geol.*, *27*, 2058–2083, doi:10.1016/j.jsg.2005.05.020.

Zoback, M. D., S. Hickman, and W. E. Ellsworth (2007), The role of fault zone drilling, in *Treatise on Geophysics*, edited by G. Schubert, pp. 649–674, Elsevier, New York.